Combustion Characteristics of MCV/LCV Fuels

- A Numerical Chemical Kinetic Study at Gas Turbine Conditions

Daniel Jarnekrans

Division of Fluid Dynamics
Department of Energy Sciences
Lund Institute of Technology
Lund University
P.O Box 118
SE-221 00 Lund
Sweden

Acknowledgements

This thesis is the final part of the Master of Mechanical Engineering Program at Lund Institute of Technology, Lund University. I had the great opportunity to do my thesis work in cooperation with Siemens Industrial Turbomachinery in Finspong, Sweden.

I would like to thank my supervisor Dr. Jenny Larfeldt for all the great support and excellent tutoring and all other persons involved at the Siemens Combustor Group.

My sincere gratitude to Professor Xue-Song Bai at Lund University for all the support and expertise provided, who has been an invaluable discussion partner during this work. I would also like to thank Changye Liu for all the assistance with the numerical work conducted in Lund.

Abstract

The purpose of this Master's Thesis is to develop a model for numerical simulations in order to kinetically characterize different *Medium Calorific- Low Calorific Value (MCV-LCV)* fuel gas mixtures. Adding fuel components with a very low heating value or inert species affect the stability of the standard gas turbine combustor design.
Siemens Industrial Turbomachinery (SIT) believes that increasing the fuel flexibility of their current gas turbine combustors is important in maintaining a leading position on the industrial power generation market.

The numerical model development has included a test of chemical reaction mechanisms suitable for modelling syngas co-fired with natural gas. Predictions of laminar flame speed and ignition delay time for various syngas fuel mixtures at different pressures and initial temperatures have been compared to experimental data. Two different reactor models suitable for ignition delay time calculations have also been evaluated. ChemKin is the primary software used in this work but a performance test of the open-source chemical kinetics code package Cantera has also been conducted for comparisons.

An investigation of the global chemical time scale, which is a fuel mixture characteristic, was performed to find a possible correlation with experimental flameout/flameback data from rig tests with a SIT burner. A correlation between the global chemical time and the limit for flameout was found for nitrogen content up to 35% by volume in the natural gas fuel for the AEV LB000 reference burner. For very high inert content in the natural gas fuel additional fluid dynamic effects becomes increasingly important, hence further confirms that the ultimate flameout limit is governed by the flow and the specific burner.

For an arbitrary burner, auto ignition in the burner mixing tube might be relevant for inducing a possible flameback. A general investigation of the ignition delay time scale has therefore been included. The risk of flameback/flashback is known to increase when adding highly diffusive species to the fuel. It is clear that auto ignition may also be a relevant mechanism in inducing/supporting a flameback, given a sufficiently high temperature for ignition. For the LB000 burner standard operating conditions, ignition delay is irrelevant due to low air preheat temperature. Ignition delay time simulations are preferably performed using a homogeneous constant-pressure reactor, determining ignition by the maximum temperature gradient.

Further development of chemical mechanisms suitable for modelling laminar flame speed and ignition delay of syngas-natural gas fuel mixtures at gas turbine operating conditions is required. The laminar flame speed predictions of ChemKin however proved quite accurate for lean mixtures at low preheat temperatures.

The open-source software Cantera has proven to be a flexible code consistently over-predicting the laminar flame speed compared to ChemKin. It is also less user-friendly due to the lack of code documentation and technical support.

Contents

Appendices

Nomenclature

Symbol	Description	Units
A'	Pre-exponential factor	$[mol, cm^{-3}, \sec^{-1}]$
A_x	Cross-sectional flow area	$[cm^{-2}]$
A_b	Flame surface area	$[cm^{2}]$
a_e	Tube wall area per length unit	$[cm]$
c	Concentration	$[mol \cdot cm^{-3}]$
C_p	Specific heat capacity	$[J \cdot kg^{-1} \cdot K^{-1}]$
D	Mass diffusion coefficient	$[m^{2} \cdot \sec^{-1}]$
D^T	Thermal diffusion coefficient	$[mol \cdot cm^{-1} \cdot \sec^{-1}]$
E_a	Activation energy	$[J \cdot mol^{-1}]$
h	Specific enthalpy	$[kJ \cdot kg^{-1}]$
k	Rate coefficient	$[mol, cm^{-3}, \sec^{-1}]$
K_c	Equilibrium constant	$[-]$
l	Integral length of turbulence	$[cm]$
$l_{f,t}$	Turbulent flame length scale	$[cm]$
L_{ig}	Auto ignition length scale	$[cm]$
L_f	Flame position	$[cm]$
$\dot{M}$	Reactant mass flow rate	$[kg \cdot \sec^{-1}]$
n	Surface normal	$[-]$
P	Pressure	$[Pa]$
Q_e	External heat flux	$[W \cdot m^{-2}]$
Q_{loss}	heat loss in system	$[W]$
Q_{source}	heat generation in system	$[W]$
$\dot{Q}$	Reactant flow rate	$[cm^{3} \cdot \sec^{-1}]$
R	Universal gas constant	$[J \cdot mol^{-1} \cdot K^{-1}]$
S_L	Laminar flame speed	$[cm \cdot \sec^{-1}]$
S_t	Turbulent flame speed	$[cm \cdot \sec^{-1}]$
t	turbulent time scale	$[sec]$
$t_{c,1}$	Critical flameback time scale	$[sec]$
$t_{c,2}$	Critical flameout time scale	$[sec]$
$t_{c,3}$	Critical ignition induced flameback time scale	$[sec]$
T	Temperature	$[K]$
u	Mean gas velocity	$[cm \cdot \sec^{-1}]$
u'	Turbulence intensity	$[cm \cdot \sec^{-1}]$
U_{sys}	Internal energy of system	$[J]$
V	Volume	$[m^{-3}]$

W	Molecular weight	$[kg \cdot kmol^{-1}]$
Y	Mass fraction	*[-]*

Superscripts

b	Temperature modifier
-	Mixture average
~	Time average
e	Educt (reactant) index
p	Product index

Subscripts

f	Forward
i	Species index
j	Reaction index
r	Reverse
s	Product or reactant index

Greek Symbols	**Description**	**Units**
α'	Thermal diffusivity	$[m^2 \cdot \sec^{-1}]$
δ_L	Laminar flame thickness	*[cm]*
ν	Stoichiometric coefficient	*[-]*
ρ	Mixture mass density	$[kg \cdot m^{-3}]$
$\dot{\omega}$	Molar rate of production	$[mol \cdot cm^{-3} \cdot \sec^{-1}]$
ϕ	Equivalence ratio	*[-]*
λ	Thermal conductivity	$[W \cdot m^{-1} \cdot K^{-1}]$
ψ	Diffusion velocity	$[cm \cdot \sec^{-1}]$
ψ_c	Correction velocity	$[cm \cdot \sec^{-1}]$
τ_{chem}	Laminar flame time scale	*[sec]*
τ_{ig}	Auto ignition time scale	*[sec]*
υ	Ordinary diffusion velocity	$[cm \cdot \sec^{-1}]$
ϖ	Thermal diffusion velocity	$[cm \cdot \sec^{-1}]$
ϑ	Binary diffusion coefficient	$[m^2 \cdot \sec^{-1}]$
Θ	Thermal diffusion ratio	*[-]*

Abbreviations

LCV	Low Calorific Value
MCV	Medium Calorific Value
API	Application Programming Interface
PFR	Plug-Flow Reactor
PSR	Perfectly-Stirred Reactor
CHR	Closed Homogeneous Reactor
FWHM	Full Width at Half Maximum

1 Introduction

1.1 Background

The necessity for increased fuel flexibility becomes more apparent in the world today where an ever increasing oil price and the green-house effect motivates the utilization of alternative process-derived gaseous fuels or different kinds of synthetic fuels for gas turbine power generation. These gaseous fuels are often produced out of coal or biomass and usually require an integrated cycle of a gasification plant and a gas turbine.
Siemens Industrial Turbomachinery in Finspong, being a part of Siemens AG is a leading manufacturer of medium-sized industrial gas turbines and believes that increasing the fuel flexibility is important in maintaining and developing its position on the gas turbine power generation market.
Burning fuels with a low heating value with high inert and or highly diffusive content, so-called *Medium- and Low Calorific Value* fuels *(MCV- and LCV fuels)* may have a profound effect on the combustor stability. LCV fuels typically originate from blast furnaces or air/oxygen blown gasification processes of coal or wood, whereas a MCV fuel might be diluted natural gas, wellhead gas or landfill gas usually with a high inert content. Burning natural gas with high concentrations of inert nitrogen, carbon monoxide or highly diffusive hydrogen may increase the risk of combustion instability phenomena such as burner *flashback* or *flameout* for lean fully premixed combustion. Flame extinction (flameout) will cause loss of power output whereas flashback may result in thermal damage and reduced life time of the combustor as the flame moves upstream into the burner mixing tube. Neither is acceptable for gas turbines used in power generation applications, where reliability and continuous operation between service overhauls is of great importance.
The chemical kinetic characteristics of natural gas fuel mixtures have been well documented. Deeper knowledge about effects of adding species such as carbon monoxide and hydrogen to natural gas is however an area of research. One research project in this field of fuel flexibility is the *Turbokraft* project, held by Lund University in cooperation with Siemens AG Finspong. The work includes both computational and experimental measurements of flow fields and turbulence in gas turbine burners burning alternative synthetic MCV/ LCV fuels.

1.2 Objectives

This work is an initial approach to numerically characterize some combustion phenomena of MCV/LCV fuel gases focusing on chemical kinetics rather than fluid dynamic characteristics of specific combustors.
The primary objective is to develop a numerical model by testing several *kinetic mechanisms* suitable for kinetic simulations of hydrogen-carbon monoxide fuel mixtures (*so-called Syngas)* co-firing with natural gas. Predictions of laminar flame speed and auto ignition delay time are to be calculated using the ChemKin software. A performance test of the chemical kinetics open-source software Cantera is also to be conducted.
The secondary objective of this work is to numerically investigate the characteristics of fuel mixtures with various compositions of hydrogen, carbon monoxide, carbon dioxide,

nitrogen and natural gas to try to find a fuel mixture-specific parameter characterizing the burner stability with respect to flashback and lean flameout at fixed flow conditions. In the general case auto ignition might also be relevant for supporting or inhibiting flashback and flameout, therefore an investigation of the ignition delay time scale will also be included.

2 Fundamentals

2.1 Introduction

This section treats some of the fundamental theory of combustion chemical kinetics, reactor models used in the simulations as well as the governing equations of one-dimensional premixed flames.

2.2 Chemical Kinetics

Chemical kinetics is the science of the interaction between chemical species. In the gas phase considered in this work, molecules of different species in a gas mixture move around and interact with each other by collisions. In a collision of two or more different molecules the intermolecular bonds may break and new chemical species are formed. This formation and consumption of chemical species is modeled using *rate laws* and *reaction mechanisms*.

2.2.1 Rate Laws

In a chemical reaction, species are formed and consumed. A general chemical reaction can be described by the equation:

$$A + B + C + ... \xrightarrow{k} D + E + F + ... \tag{1}$$

Where $A, B, ...$ denote the *reactant* species reacting into the *product* species $D, E...$
A rate law describes an empirical formulation of the *reaction rate* by which the species are formed or consumed. The consumption rate of the reactant *A* can be expressed as

$$\frac{d[A]}{dt} = -k_f \cdot [A]^{n_1} \cdot [B]^{n_2} \cdot [C]^{n_3} \cdot ..... \tag{2}$$

The exponents $n_1, n_2, n_3, ...$ are the *reaction orders* with respect to $A, B, ...$ and *k* is the *rate coefficient* with [] brackets denoting the molar concentration. The rate coefficient can be described by the so-called *Arrhenius law*

$$k_f = A' \cdot T^b \cdot e^{\left(-\frac{E_a}{RT}\right)} \tag{3}$$

Here A' is *a preexponential factor*, *b* a temperature modifier exponent and E_a the *activation energy*. These parameters are all determined experimentally. *R* is the universal gas constant and *T* is the temperature.

For the reverse reaction of equation (1) the rate law for production of is

$$\frac{d[A]}{dt} = k_r \cdot [D]^{n_4} \cdot [E]^{n_5} \cdot [F]^{n_6} \cdot ..... \tag{4}$$

At chemical equilibrium the production and consumption of a species equals which results in the so-called *equilibrium constant* K_c defined as

$$K_c = \frac{k_f}{k_r} = \frac{[D]^{n_4} \cdot [E]^{n_5} \cdot [F]^{n_6} \cdot \ldots}{[A]^{n_1} \cdot [B]^{n_2} \cdot [C]^{n_3} \cdot \ldots} \tag{5}$$

2.2.2 Elementary Reactions

An *elementary reaction* is a chemical reaction that occurs exactly in the way which is described by the reaction equation of that reaction. An example of an elementary reaction could be:

$$OH + H_2 \rightarrow H_2O + H \tag{6}$$

The OH radical reacts with the hydrogen molecule and instantly form a water molecule H_2O and a hydrogen radical *H*. These reactions take place through *reactive* collisions of the molecules in the gas. In some cases the collisions are *non-reactive* where the molecules collide and bounce apart and no reaction takes place. A non-elementary reaction could be:

$$2H_2 + O_2 \rightarrow 2H_2O \tag{7}$$

Detailed investigations show that water is not formed from hydrogen and oxygen in one single step but with several intermediate steps where intermediate species like *OH, H* and *O* are formed. Reaction (7) is usually called a *net reaction* or *global reaction* of the formation of, in this case water.
The elementary reactions can occur in different ways. *Unimolecular* reactions describe the rearrangement or dissociation of a molecule:

$$A \rightarrow products \tag{8}$$

Such reactions have a first-order rate law, thus if the initial concentration is doubled, the reaction rate is also doubled.
Bimolecular reactions are the most common ones, proceeding according to

$$A + B \rightarrow products \tag{9}$$

Or

$$A + A \rightarrow products \tag{10}$$

Bimolecular reactions have a second-order rate law. A doubling of the concentration of each reaction partner quadruples the reaction rate.
Trimolecular reactions obey a third-order rate law and are usually recombination equations like

$$
\begin{aligned}
&A + B + C \rightarrow products \\
&A + A + B \rightarrow products \\
&A + A + A \rightarrow products
\end{aligned}
\tag{11}
$$

2.2.3 Reaction Mechanisms

In combustion numerous elementary reactions occur simultaneously and depend on each other in a coupled manner, each with different rate coefficients. The equation of an arbitrary elementary reaction *j* involving *S* species is given by:

$$
\sum_{s=1}^{S} \nu_{js}^{(e)} A_s \overset{k}{\rightarrow} \sum_{s=1}^{S} \nu_{js}^{(p)} A_s \tag{12}
$$

Here $\nu_s^{(e)}, \nu_s^{(p)}$ denote the stoichiometric coefficients of the reactant *s* (also called *educts*) and the products respectively with *s=1,...,S.* A_s is the chemical formula of species *s.*

The rate law for the formation of species *i=1,...,S* in <u>one</u> particular reaction can be written as:

$$
\left(\frac{\partial c_i}{\partial t} \right) = k_f \left(\nu_i^{(p)} - \nu_i^{(e)} \right) \prod_{s=1}^{S} c_s^{\nu_s^{(e)}} \tag{13}
$$

The total rate of formation of a species *i* is given by the summation over the rate equations of all elementary reactions *j=1,...,N* [1].

$$
\left(\frac{\partial c_i}{\partial t} \right) = \sum_{j=1}^{N} k_{f,j} \left(\nu_i^{(p)} - \nu_i^{(e)} \right) \prod_{s=1}^{S} c_s^{\nu_s^{(e)}} \tag{14}
$$

Equation 14 forms a system of non-linear ordinary differential equations that has to be solved in time simultaneously for all species *i=1,...,S* and describes the path the different reactants take when reacting into products. The parameters in this ODE-system form a so-called *chemical kinetic mechanism.*

2.3 Reactor Theory

The well-stirred chemical reactor can be described as a control volume where a gas mixture is allowed to equilibrate under perfectly homogeneous conditions. The concept of the well-stirred reactor is applicable to calculations of ignition delay time. The governing equations of different reactor models are therefore introduced here.

2.3.1 Plug-Flow Reactor

In the ideal *plug-flow reactor (PFR)* or *tube reactor* no recirculation occurs and the flow is homogeneous with respect to velocity and species concentration in a radial

direction from the axis of symmetry. The physical interpretation is that the flow is trapped in between two membranes/pistons that move with the same velocity as the flow along the tube, thus inhibiting any recirculation/mixing in the axial direction of the tube [2].

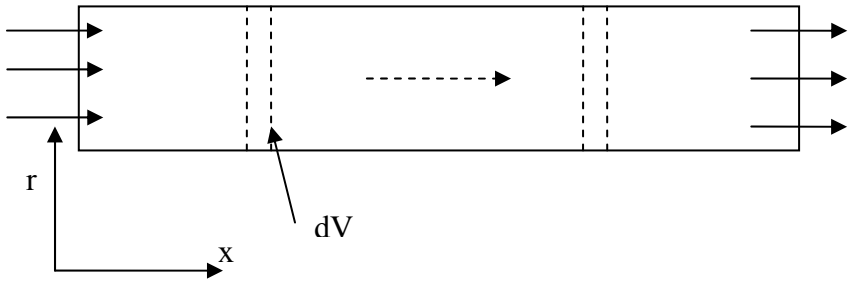

Figure 1. Schematic plug-flow reactor

There is a clear analogy to an ideal perfectly mixed mixing tube of a gas turbine burner; motivating the use of this reactor model in this work.
For the plug-flow reactor some assumptions can be made for ignition delay applications:

- Steady state, one-dimensional flow
- Only gas-phase reactions
- Ideal gas behaviour
- Ideal frictionless flow

Applying the above simplifications the mass conservation equation can be written as

$$\rho u \frac{dA_x}{dx} + \rho A_x \frac{du}{dx} + u A_x \frac{d\rho}{dx} = 0 \tag{15}$$

Here ρ is the mixture mass density and u the velocity of the gas which consists of S species. A_x is the cross-sectional flow area. The conservation of species can be formulated as

$$\rho u A_x \frac{dY_i}{dx} = W_i \dot{\omega}_i A_x \tag{16}$$

W_i is the molecular weight of species i and $\dot{\omega}_i$ is the molar rate of production (see Eq. 13) of species i. The energy equation is formulated as

$$\rho u A_x \left(\sum_{i=1}^{S} h_i \frac{dY_i}{dx} + \overline{C}_p \frac{dT}{dx} + u \frac{du}{dx} \right) = a_e Q_e \tag{17}$$

h_i is the specific enthalpy of species *i*, $\overline{C}_p$ the mean heat capacity per unit mass of gas, Q_e the heat flux from the surroundings to the outer wall of the tube whose area per length unit is a_e [3].

The **initial conditions** are:

$$Y_i(x=0) = Y_{i,0}$$
$$T(x=0) = T_0$$

2.3.2 Closed Homogeneous Reactor

The *closed homogeneous reactor (CHR)* is a spherical reactor containing a perfectly mixed gas, allowed to react starting from an initial time t_0. The inner shell is allowed to expand and increasing the volume, enable reactions to occur at constant pressure.

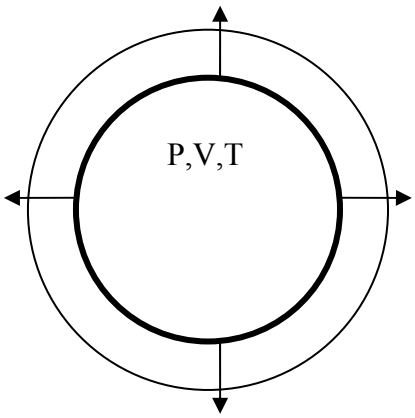

Figure 2. Schematic of a closed homogeneous constant pressure reactor.

The closed homogeneous reactor requires, apart from infinitely fast mixing, many other assumptions and simplifications for ignition delay applications.

- Mass transport is assumed infinitely fast
- No inflow or outflow
- Only gas-phase reactions
- Ideal gas behaviour
- (Ideal frictionless flow)

The mass conservation equation becomes

$$\frac{d}{dt}(\rho V) = 0 \tag{18}$$

where $V = V(t)$ is the volume.

Conservation of species

$$\left(\rho_i V\right)\frac{dY_i}{dt} = W_i\left(\dot{\omega}_i V\right) \tag{19}$$

And finally the gas energy equation

$$\frac{dU_{sys}}{dt} = -Q_{loss} + Q_{source} - P\frac{dV}{dt} \tag{20}$$

Where U_{sys} is the total internal energy, Q_{loss} is the net outward heat flux and Q_{source} is the heat generated in the reactor [3].

The **initial conditions** are:

$Y_i(t=0) = Y_{i,0}$
$V(t=0) = V_0$

2.4 1-D Laminar Premixed Flames

The premixed laminar flame on a flat burner can be treated as one-dimensional and is therefore attractive for numerical modelling. An idealized flat burner as shown in Figure 3 is a flat burner with infinite flow cross-sectional area. By only considering the flame far away from the boundaries the laminar flame has one-dimensional properties, hence only varies in the x-direction.

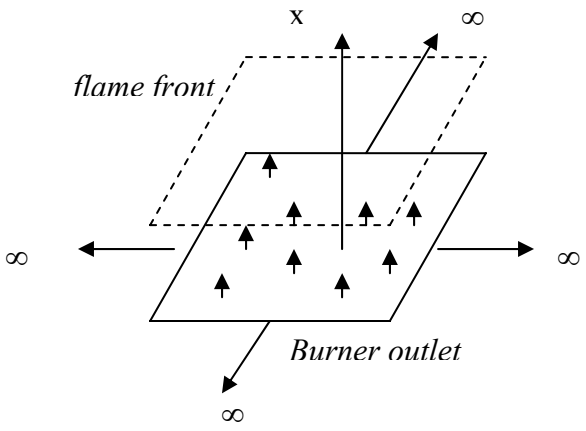

Figure 3. A schematic of flat burner with infinite cross-sectional outlet area.

In deriving the conservation equations for a simple one-dimensional flame some approximations are made:

- The gas is modeled as ideal.
- Effect of gravitation is neglected.
- The molecular mean free path is small in relation to the flame thickness, hence a continuous system.
- Constant pressure.
- The kinetic energy of the gas is neglected; no shock waves are considered.
- No radiation effects are included, hence a non-sooting flame.
- Local thermal equilibrium of the system.

The derivation of the general equations for a one-dimensional flame is trivial; hence the resulting equations are only presented below.

$$\text{Continuity} \qquad \frac{\partial \rho}{\partial t} + \frac{\partial (\rho u)}{\partial x} = 0 \tag{21}$$

$$\text{Species conservation} \qquad \rho \frac{\partial Y_i}{\partial t} = \frac{\partial q_i}{\partial x} - \rho u \frac{\partial Y_i}{\partial x} + \dot{\omega}_i \tag{22}$$

$$\text{Energy Equation} \quad \rho C_p \frac{\partial T}{\partial t} = \frac{\partial}{\partial x}\left(\lambda \frac{\partial T}{\partial x} \right) - \left(\rho u C_p + \sum_{i=1}^{S} q_i C_{p,i} \right) \frac{\partial T}{\partial x} - \sum h_i \dot{\omega}_i \tag{23}$$

where x is the spatial coordinate, t denotes time, T is the temperature, ρ is the total mass density, u is the mean flow velocity, Y_i is the mass fraction of species *i*, $q_i = \rho Y_i \psi_i$ is the diffusion flux of species *i* with ψ_i being the diffusion velocity, C_p the constant pressure specific heat, h_i specific heat of species *i* and λ is the thermal conductivity of the mixture [1]. The continuity equation states that the total mass of the system is preserved. The species conservation equation states that the species concentration is balanced by the diffusion of and production/consumption of chemical species into the system and convective transport of species out of the system. The energy equation states that the overall energy of the system is controlled by heat conduction (1st term on the right hand side of eq 23), convective and diffusive heat transport (2nd term on the right hand side of eq 23) and energy generated or consumed by the chemical kinetic reactions (3rd term of eq 23).
The governing equations are to be solved with respect to the flow velocity *u* to obtain the laminar burning velocity of the flame. Further numerical details, boundary conditions and system closure can be found in section 5.4.2.

3 Burner Stability

A stable premixed flame requires that the flame velocity is equal and opposite of the reactant gas velocity. In a gas turbine burner the flow velocity is generally much higher than the flame speed therefore the flame is stabilized by generating high inlet swirl which causes recirculation of the product gases[4]. A schematic of a swirl-stabilized burner is shown in Figure 4. At the flame front of a fully turbulent stabilized flame:

$$\begin{aligned} \vec{u} \times \vec{n} &\sim S_L \quad \text{(instant)} \\ \tilde{\vec{u}} \times \tilde{\vec{n}} &\sim S_t \quad \text{(mean)} \end{aligned} \tag{24}$$

where the instantaneous turbulent flow velocity is decomposed as $\vec{u} = \tilde{\vec{u}}(x,y,z,t) + \vec{u}'(x,y,z,t)$. $\tilde{\vec{u}} = \tilde{\vec{u}}(x,y,z,t)$ is the time-averaged turbulent flow velocity and $\vec{u}' = \vec{u}'(x,y,z,t)$ the fluctuating component. S_L, S_t denote the laminar and turbulent flame speed respectively.

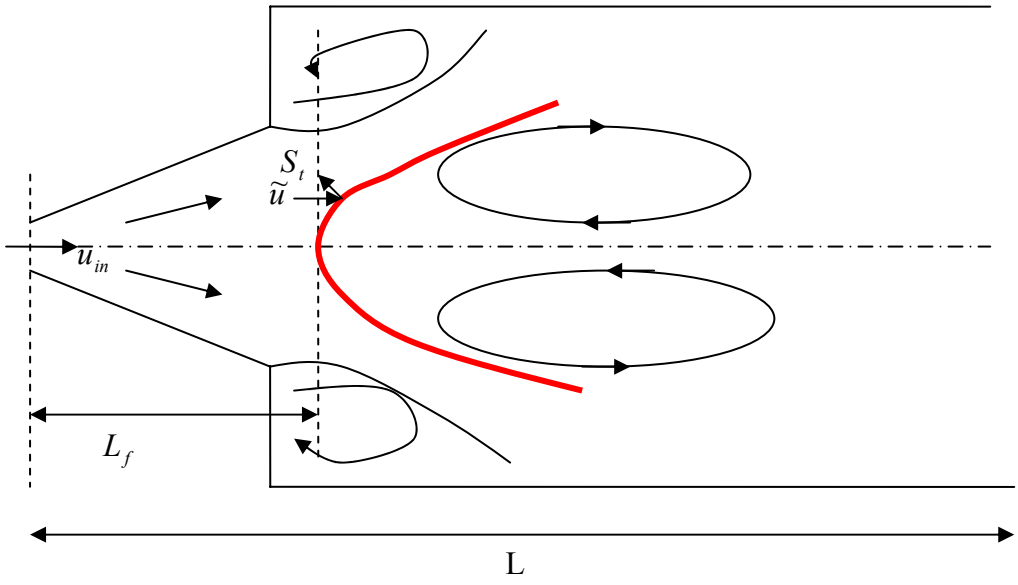

Figure 4. Schematic view of the flame front with recirculation zones in a typical swirl-stabilized burner.

In reality a turbulent flame front is not very smooth, rather wrinkled as illustrated in Figure 5.

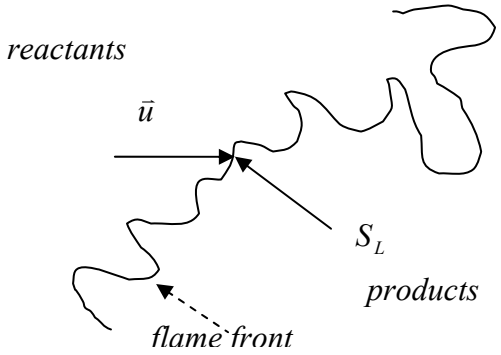

Figure 5. Close-up view of a turbulent wrinkled flame front at one instant.

A relevant turbulent time scale of the flow at a given point would be

$$t \cong \frac{l}{\tilde{u}} \tag{25}$$

where l is the integral length of the turbulence and $\tilde{u}$ is a characteristic mean flow velocity

At the flame front the turbulent flame length scale $l_{f,t}$ is in the same order of magnitude as the integral length scale *l*:

$$l_{f,t} \cong l \tag{26}$$

The turbulent flame speed is typically related to the laminar flame speed through a correlation of the form

$$\frac{S_t}{S_L} = f(u', S_L) \tag{27}$$

where u' is the turbulence intensity, ϕ is the equivalence ratio and $S_L = f(P, T, \phi, fuel)$ is the laminar flame speed. According to Equations (24), (25) and (26) at a given point at the flame front:

$$\frac{l_{f,t}}{S_t} \sim \frac{l}{\tilde{u}} \Rightarrow t_{f,t} \sim t \tag{28}$$

This means that if the turbulent flow time is in the same order as the turbulent flame time scale the flame is stabilized in the burner. Turbulent flame time can be related to the laminar flame time scale as follows

$$t_{f,t} = \frac{l}{S_t} \sim \frac{l}{S_L \times f(u', S_L)} = \frac{l}{f(u', S_L) \times \delta_L} \times \frac{\delta_L}{S_L} \sim \frac{l}{f(u', S_L) \times \delta_L} \cdot \tau_{chem} \quad (29)$$

where δ_L is the laminar flame thickness and τ_{chem} is the laminar chemical kinetic time scale. It appears that

$$t_{f,t} \propto \tau_{chem} \quad (30)$$

Flameback (flashback) can occur in the burner mixing tube if the local flow speed is lower than the flame speed, i.e.

$$u_{in} < S_t \quad (31)$$

Define a critical time scale of the burner as

$$t_{c,1} \equiv (l/u_{in})/(l/(f(u', S_L) \times \delta_L)) = f(u', S_L) \times \delta_L / u_{in} \quad (32)$$

From Equations (29), (30) and (31) flame back occurs if

$$\tau_{chem} < t_{c,1} \quad (33)$$

Similarly, flameout (blowout) in the burner can occur if the local flow speed is higher than the flame speed, i.e.

$$u_{combustor} > S_t \quad (34)$$

Vortex breakdown causes the flow reversal at the outlet of the burner mixing tube (see Figure 4), thus Eq. (34) is typically not a realizable condition. This will generate a stabilized flame without risk of flameout unless the flow speed is extremely high. If the flow speed in the burner is too high then the level of turbulence will be too high and the turbulent length scales will be very small as well. This will cause flame extinction and eventually blowout completely. This flameout flow velocity $u_{flameout}$ defines a second critical time scale of the burner.

$$t_{c,2} \equiv (l/u_{flameout})/(l/(f(u', S_L) \times \delta_L)) = f(u', S_L) \times \delta_L / u_{flameout} \quad (35)$$

From equations (29), (34) and (35) flameout occurs if

$$\tau_{chem} > t_{c,2} \quad (36)$$

For a given burner, since the cross-sectional area of the burner outlet is larger than the burner mixing tube (see Figure 4)

$$u_{combustor} < u_{in}$$

This leads to

$$t_{c,2} > t_{c,1} \tag{37}$$

A stable flame requires

$$t_{c,1} < \tau_{chem} < t_{c,2} \tag{38}$$

Auto ignition will under certain conditions affect the stability range of a given burner. If auto ignition occurs in the burner mixing tube a flame back might be initiated.
The auto ignition delay length scale can be defined as

$$L_{ig} \equiv u_{in}\tau_{ig} \tag{39}$$

where u_{in} is the mean axial flow velocity in the burner mixing tube and t_{ig} the ignition delay time of the fuel-air mixture. Auto ignition may occur upstream if

$$L_{ig} < L_f \tag{40}$$

where L_f is the position of the flame measured from the inlet and approximately equal to the length of the mixing tube. Define a third critical burner time scale

$$t_{c,3} \equiv L_f / u_{in} \tag{41}$$

The criterion for flame back to occur Eq.(40) can be reformulated as:

$$\tau_{ig} < t_{c,3} \tag{42}$$

In conclusion, flameback may occur if one of the following criterions is satisfied

$$\tau_{ig} < t_{c,3}, \qquad or \qquad \tau_{chem} < t_{c,1} \tag{43}$$

And flameout may occur if

$$\tau_{chem} > t_{c,2} \tag{44}$$

As seen, the three burner-critical time scales are burner specific thus, depending on the burner geometry, swirl conditions and cooling conditions. From their definition, it appears that they also depend (likely weakly) on the laminar flame speed S_L and flame thickness δ_L.
According to the above formulation, an investigation of the laminar flame time scale τ_{chem} and ignition delay time τ_{ig} may be sufficient to determine the combustion

behaviour of an arbitrary burner when burning different fuels. This motivates the current study of these two chemical time scales [5].

4 Global Chemical Time Scale

4.1 Definitions

There are various ways to define a global chemical time scale for laminar flames. One common approach is the flame propagation model of Zeldovich where the so-called *Lewis number* is assumed to be unity $Le = \frac{\alpha'}{D} = 1$. α' is the thermal diffusivity of the mixture and *D* is the mass diffusivity. The chemical time is approximated as [1],[6],[7]

$$\tau_{chem} = \frac{\alpha'}{S_L} \tag{45}$$

The assumption of a Lewis number close to unity is however no longer valid when introducing highly diffusive species such as hydrogen in the gas mixture.
A more physically reasonable and general approximation of a global chemical time scale would be (following Eq. (29) and (35))

$$\tau_{chem} \cong \frac{\delta_L}{S_L} \tag{46}$$

where $\delta_L = f(T, P, \phi, fuel)$ is the laminar flame thickness.

4.2 Flame Thickness

The thickness of a premixed laminar flame or the thickness of the reaction zone can be determined using the *FWHM (Full Width at Half Maximum)* [8] approach on the gradient of the temperature profile of the flame.

Consider the temperature solution of a laminar premixed flame as shown in Figure 6. Here the reactor domain length is set to 5 cm and the preheat temperature $T_u = 300K$.

The flame thickness δ_L is calculated as the width at half of the maximum value of the temperature gradient $\frac{dT}{dx}$ as shown in Figure 7.

With the inverse function $\hat{x} = \hat{x}(\frac{dT(x)}{dx})$ the flame thickness is calculated as

$$\delta_L = \hat{x}(0.5 \cdot \max\left(\frac{dT}{dx}\right))_2 - \hat{x}(0.5 \cdot \max\left(\frac{dT}{dx}\right))_1 \tag{47}$$

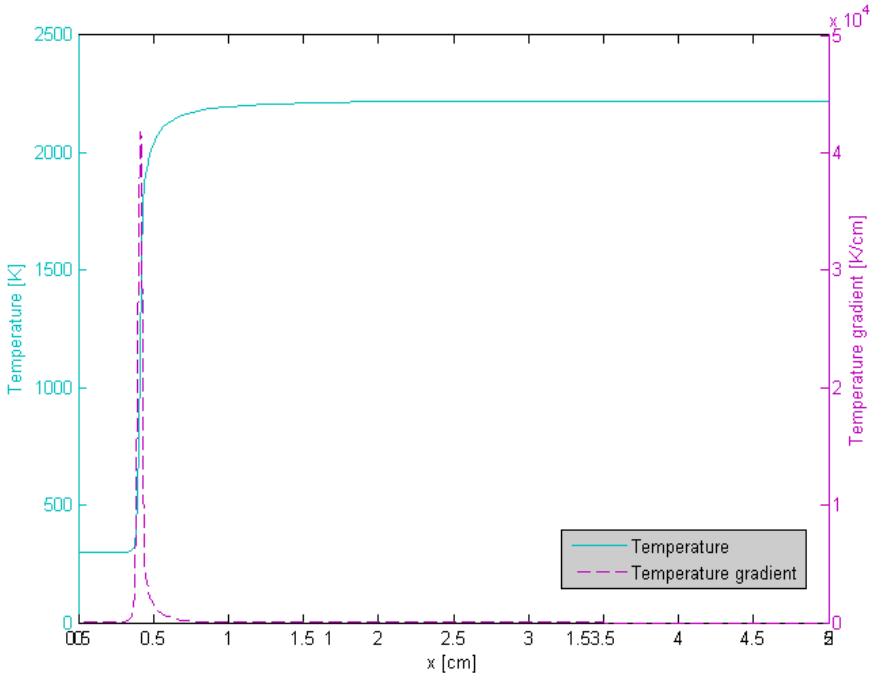

Figure 6. A typical temperature profile of with corresponding temperature gradient for a laminar premixed flame.

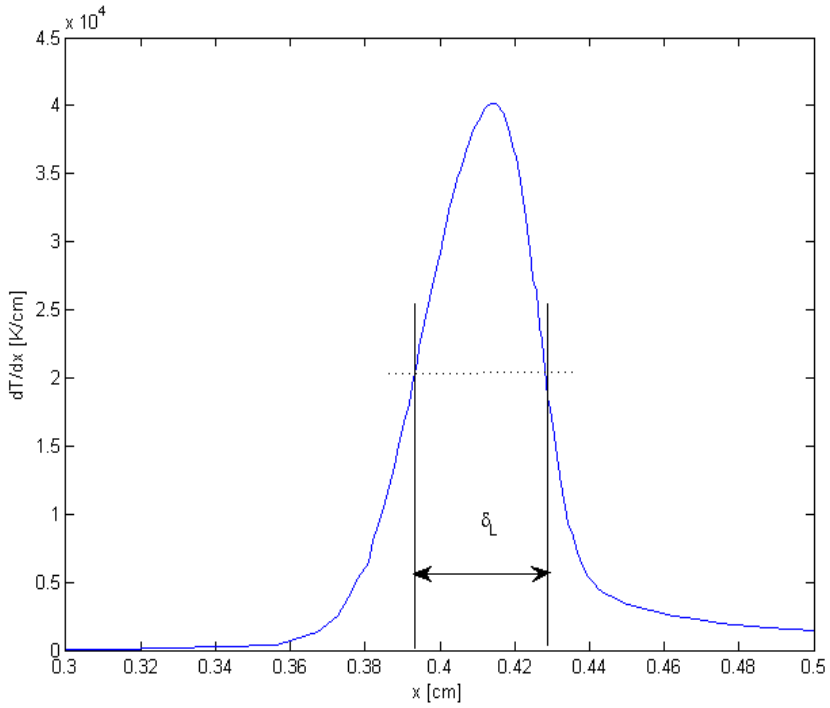

Figure 7. A close-up view of the temperature gradient showing the definition of the flame thickness according to FWHM

5 Model Setup - Selecting a Reaction Mechanism

5.1 Introduction

In this section the mechanisms of interest are tested by comparing predicted laminar flame speeds and auto ignition delay times against existing experimental data found in the literature. The objective is to find discrepancies, focusing on H2/CO fuel mixtures at pressures and inlet temperatures representative of gas turbine running conditions. Comparisons between the predictions of ChemKin and Cantera are also made.

5.2 Mechanisms

A review of recent work in the literature was conducted resulting in three mechanisms for further evaluation containing at least methane or higher order hydrocarbon species since simulations of co-firing syngas with methane/natural gas are to be performed further ahead. The table below show some of the chemical kinetic mechanisms found in the literature.

Table 1 A summary of some kinetic mechanisms found in the literature. The ones included in the test in bold face.

Mechanism	No. of species	No. of reactions	C-Order
Davis et al. [9]	14	30	1
Sun et al. [10]	13	33	1
Li et al. [11]	18	84	1
Skreiberg et al. [12]	73	400	2
GRI 3.0 [13]	53	325	3
Williams et al (San Diego) [14]	46	234	3
Konnov [15]	127	1200	6

The three mechanisms included in the selection process are further described below.

The GRI 3.0 mechanism [13] developed by The University of California Berkeley, Standford University, The University of Texas at Austin and SRI International, is a detailed model with 53 species and 325 reaction steps and is optimized and thoroughly tested and validated for natural gas fuel blends, thus acting as a reference. The mechanism contains hydrocarbon species of C3 and lower. The optimization is based on laminar flame speed data up to 20 atm. pressure and ignition delay data up to 84 atm. pressure.

The mechanism of Skreiberg et al [12] is a detailed mechanism originally developed for ammonia oxidation in the presence of methane, hydrogen and carbon monoxide, hence also somewhat suitable for syngas combustion co-firing with methane. It contains 73 species and more than 400 reaction steps with hydrocarbon species of C2 and lower. The optimization is however focused on fuel-rich conditions and moderate temperatures below 1400 K.

The mechanism of Williams et al [14] is a smaller detailed model containing 46 species and 234 reaction steps with hydrocarbon species of C3 and lower. The sub mechanism for hydrogen and carbon monoxide combustion was updated and optimized in 2006 [16]. In this model, attention is restricted to pressures below 100 bar, equivalence ration less than 3 and temperatures above 1000 K which suits the purpose of simulating gas turbine conditions. This mechanism is also optimized for natural gas.

5.3 Experimental data

Extensive work has been done on the combustion behaviour of natural gas blends; however the amount of experimental data on syngas-air flames at elevated pressures and lean fuel mixtures typical of gas turbine running conditions is not very extensive although some measurements do exist.

Laminar flame speed measurements on a conical Bunsen flame by Natarajan et al [17] for both atmospheric and elevated pressures were used. The effect of flame stretch has been limited by making the flame speed calculations based on the reaction zone area unlike many previous attempts, where the flame surface area has been used.

$$S_{L,u} = \dot{Q} / A_b \tag{48}$$

$\dot{Q}$ is the volumetric reactant flow rate of the Bunsen burner and A_b the flame reaction zone area. The reaction zone area was determined from a chemiluminescence emission image using an edge detection program. The image was produced through averaging over 25 frames.

Recent work by Sun et al [10] includes laminar flame speed measurements using the constant-pressure spherical flame technique with an outwardly propagating flame for various CO/H2/air and CO/H2/He mixtures at pressures up to 40 atmospheres. The time resolved schlieren images were recorded using a high-speed digital camera.
For the high pressure experiments, helium was used as a diluent to maintain flame stability. The effect of flame stretch has not been accounted for.

Data from the work of Mclean [18] was used to further test the mechanisms at atmospheric pressure. The flame speed measurements were conducted using a spherical bomb. The flame propagation was recorded using high-speed cine-photography of the schlieren image.

Some laminar flame speed data of methane-air mixtures from the work of Andrews and Bradley [19] was used for comparison.

The work of Petersen et al[20] includes measurements from a shock tube facility of auto ignition delay times with experiments performed behind reflected shock waves was also utilized. The ignition times were measured using the combination of a pressure transducer and a photomultiplier tube detector monitoring CH* radical chemiluminescence.

All the experimental data used in the test process is summarized in Table 2.

Table 2 A summary of the experimental data used in the model setup.

	Author:	Experimental setup	Tu [K]	P	Fuel Range	Oxidizer
					H2:CO	
Laminar Flame Speed	Natarajan et al. [17]	Bunsen Burner	300-700	1-15 atm	20:80-80:20	Air, O2:He
	Mclean et al. [18]	Spherical Bomb	300	1 atm	50:50	Air
	Sun et al. [10]	const. P Bomb	298	1-40 atm	5:95-50:50	Air, O2:He
	Andrews & Bradley [19]		300	1atm	CH4	Air
					CH4:H2	
Ignition Delay	Petersen et al. [20]	Shock-tube	1290-2000	0.5-25 atm	80:20:00 60:40:00	Air

5.4 Numerical Model

5.4.1 The ChemKin Software Package

The ChemKin 4 package is a chemical kinetics software used for simulations of elementary gas-phase and surface chemical kinetics based on the ChemKin II code originally developed by Sandia National Laboratories, Livermore California.
It consists of three major parts:

- A chemical mechanism interpreter
- Reactor Models and tools
- A post-processor for visualization of results

The interpreter or pre-processor is used to initialize the chemical mechanism with corresponding thermodynamic- and transport properties.
There is a large choice of different reactor models addressing industry-specific reacting-flow conditions in chemical processing as well as in combustion science. Results are visualized using the post-processor. Post-processing or manipulation of data can also be done externally through the *CHEMKIN Application Programming Interface* (CHEMKIN API) with C++ or Fortran programming.
Among the well-stirred reactors; closed homogeneous, partially stirred and different plasma reactors can be found. A plug-flow reactor along with models for laminar flame simulations, shock-tubes and an IC-engine are also available. Apart from all the reactor models additional tools for building reactor networks are also included. A reactor network can be constructed by means of “drag n’ drop” of different components in a diagram.

5.4.2 1-D Flame Equations in ChemKin

Here the mathematical model of the freely propagating laminar flame of ChemKin is presented. The PREMIX [3] module solves the one-dimensional flame equations from section 2.4 with some additional approximations:

- Adiabatic conditions, hence no heat loss to surroundings.
- Uniform inlet conditions, hence homogeneous fuel-oxidizer mixture.

With the assumptions above the governing equations are reduced to:

$$\dot{M} = \rho u A_x \tag{49}$$

$$\dot{M}\frac{dY_i}{dx} + \frac{d}{dx}\left(\rho A_x Y_i \psi_i\right) - A_x \dot{\omega}_i W_i = 0 \qquad (i = 1,....,S) \tag{50}$$

$$\dot{M}\frac{dT}{dx} - \frac{1}{C_p}\frac{d}{dx}\left(\lambda A_x \frac{dT}{dx}\right) + \frac{A_x}{C_p}\sum_{i=1}^{S}\dot{\omega}_i h_i W_i = 0 \tag{51}$$

$$\rho = \frac{P\overline{W}}{RT} \tag{52}$$

Here x denotes the spatial coordinate, $\dot{M}$ the mass flow rate and $\overline{W}$ the mean molecular weight of the mixture.
$\dot{\omega}_i$ is the molar rate of production and results from the chemical kinetics of that species where each reaction is modelled using a modified Arrhenius equation (section 2.2.3):

$$k = A' T^b \exp\left(\frac{-E_a}{RT}\right) \tag{53}$$

For **mixture-averaged** transport properties the diffusion velocity is composed of:

$$\psi_i = \upsilon_i + \varpi_i + \psi_c \tag{54}$$

Where the ordinary diffusion velocity is given by:

$$\upsilon_i = D_{im}\frac{1}{X_i}\frac{dX_i}{dx} \tag{55}$$

Where X_i is the mole fraction and the mixture-averaged diffusion coefficient is given in terms of the binary diffusion coefficient ϑ_{ik} of species *i* diffusing into species *k*:

$$D_{im} = \frac{1 - Y_i}{\sum_{k \neq i}^{S} X_k / \vartheta_{ik}} \tag{56}$$

The thermal diffusion velocity is included for low molecular weight species:

$$\varpi_i = \frac{D_{im} \Theta_i}{X_i} \frac{1}{T} \frac{dT}{dx} \tag{57}$$

where Θ_i is the thermal diffusion ratio. The sign of Θ_i makes the lower weight species diffuse from low to high temperature regions.
The correction velocity ψ_c is included to insure that the mass fractions sum to unity, hence:

$$\sum_{i=1}^{S} Y_i \psi_i = 0 \tag{58}$$

For **multi-component** transport properties the correction velocity ψ_c is not required and the diffusion velocity is therefore defined as

$$\psi_i = \upsilon_i + \varpi_i \tag{59}$$

with the ordinary diffusion velocity term

$$\upsilon_i = \frac{1}{X_i \overline{W}} \sum_{k \neq i}^{S} W_k D_{i,k} d_k \tag{60}$$

$\overline{W}$ is the mean molar mass, W_k the mean molar mass of species *k* and

$$d_k = \nabla X_i + (X_i - Y_i) \frac{1}{P} \nabla P \tag{61}$$

The thermal diffusion velocity is

$$\varpi_i = \frac{D_i^T}{\rho Y_i} \frac{1}{T} \nabla T \tag{62}$$

Where D_i^T is the thermal diffusion coefficient for species *i*.

The **boundary conditions** are:

Dirichlet conditions at the cold boundary

$$\begin{aligned} T(x = 0) &= T_u \\ Y_i(x = 0) &= Y_{i,0}, \forall i = 1,...,S \end{aligned} \tag{63}$$

Neumann conditions at the hot boundary

$$\left.\frac{dT}{dx}\right|_{x=x_1} = 0$$
$$\left.\frac{dY_i}{dx}\right|_{x=x_1} = 0, \forall i = 1,...,S \tag{64}$$

The massflow $\dot{M}$ is an eigenvalue of the solution for freely propagating flames and must therefore be determined as a part of the solution.
The additional constraint is therefore to fix the location of the flame by specifying and fixing the temperature at one point in such a way that the temperature and species gradients 'vanish' at the cold boundary when the problem is solved. If not done properly, there will be a heat flux at the cold boundary resulting in a too low $\dot{M}$ [3].

$$T(0 < x_{fix} < x_1) = T_{fix} \tag{65}$$

$$T_u < T_{fix} < T_b \tag{66}$$

A hybrid time-integration Newton-iteration scheme is used to solve the steady state mass, species and energy conservation equations (eq. 49, 50 and 51). The laminar flame speed is defined as the mean gas velocity at the cold boundary, hence:

$$S_L = u(x = 0) \tag{67}$$

Figure 8 show the spatial temperature solution profile of a typical laminar flame with the inlet mass flow $\dot{M}$ of the reactants from the left and the flame propagating from right to left with the laminar burning velocity S_L.

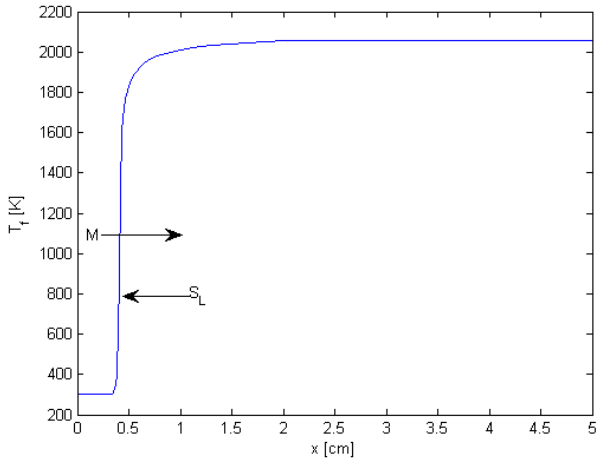

Figure 8. The one-dimensional domain with the temperature solution of an arbitrary flame

5.4.3 Method - ChemKin

The laminar flame speed predictions were calculated using the PREMIX code [3]. The default domain size was set to be 10 cm with the adaptive grid parameters (GRAD and CURV) ultimately set to 0.1 through 3 steps of refining the grid using *continuations*, solving the problem on a coarse grid and then a successive refinement for each continuation. Some alterations of the node distribution on the initial coarse grid had to be made due to convergence issues when running at high pressure. An approximate temperature profile had to be provided as an initial guess for the solver. The effect of thermal diffusion was included since hydrogen is a very light species and sensitive to temperature. Mixture-averaged transport properties were used in the simulations to reduce computational time.
Species-specific transport properties could however be considered important in the case of high H2 content in the fuel mixture since hydrogen also have a very high mass diffusivity compared to carbon monoxide, oxygen and nitrogen. A comparison of both methods can be seen in Figure 17. For species mass conservation closure, the correction velocity formulation was used to distribute the error over all species. An optional approach would be to use the trace species approximation, treating abundant species as diluents. Since the investigations not only treat lean mixtures but also stoichiometric mixtures this is considered too inaccurate.
The original discretization scheme for the convective mass flux terms as opposed to the new scheme, requiring more detailed species profiles and grid resolution points for convergence, was used.

Simulations of ignition delay times were performed using the *Plug-Flow reactor* and the *Closed Homogeneous constant-pressure reactor* models in ChemKin.
In the plug-flow reactor the ignition time was calculated by determining the distance travelled of the gas in the tube for a fixed axial gas velocity. The ignition distance was determined through the maximum gradient of the temperature and also by local maximum of OH and HO2 radical species concentration. An example of a solution in terms of OH and HO2 species concentration and further discussion regarding the differences in the ignition definition is made in section 5.5.1 p. 34-36.
For the closed homogeneous reactor, the ignition time was also determined by calculating the temporal point at which the maximum temperature gradient was located and by determining local maximum of radical species concentration. Comparisons of OH and HO2 radical peak times with max temperature gradient times were made.
The use of the *PSR* (*Perfectly-Stirred Reactor)* model, which might be physically representative of the recirculation of the fuel mixture in a gas turbine burner, has been excluded since it has been proven to produce the same results as a *PFR* for methane-based fuels. Further details can be found in the work of Tillmark [21].

5.4.4 Method - Cantera

For the flame speed calculations with the Cantera code, a program with the same basic features as PREMIX was used. The Cantera class for a freely propagating flame use a solver similar to the one in PREMIX. The velocity at every point in the domain is obtained and the overall laminar flame speed is defined as the velocity at the point on the cold boundary.

A temperature profile was specified for the solver with the gradient and curvature ratios set to 0.2 and 0.02 respectively.
For the ignition delay time calculations a homogeneous constant pressure reactor class from the Cantera package was used. A simple program was written to set up the reactor and specify fuel composition. Any further details regarding the numerical methods used in the solver have not been found since Cantera is an open-source software package.

5.5 Mechanism Selection – Results & Analysis

The results of the simulations performed with the three mechanisms with parameters taken from the experimental literature are shown below. Comparisons between predicted results of the simulations and the experimental data are made of laminar flame speeds and ignition delay time.

5.5.1 ChemKin Simulations

For laminar flame speed predictions of lean fuel mixtures, all the mechanisms seems to agree quite well for a binary mixture of H2 and CO in air at atmospheric conditions as can be seen in Figure 9.
The mechanism of Skreiberg et al. slightly over predicts the flame speed compared to measurements whereas the mechanism of Williams et al. has the best fit. A diverging trend can be seen for increasing equivalence ratio. The GRI-mechanism as well as Skreiberg over predicts the flame speed at equivalence ratios close to $\phi = 2$. Comparing the maximum laminar flame speed of syngas and pure methane-air mixtures, it is clear that it differs by almost a factor of 5 at atmospheric conditions. In the gas turbine

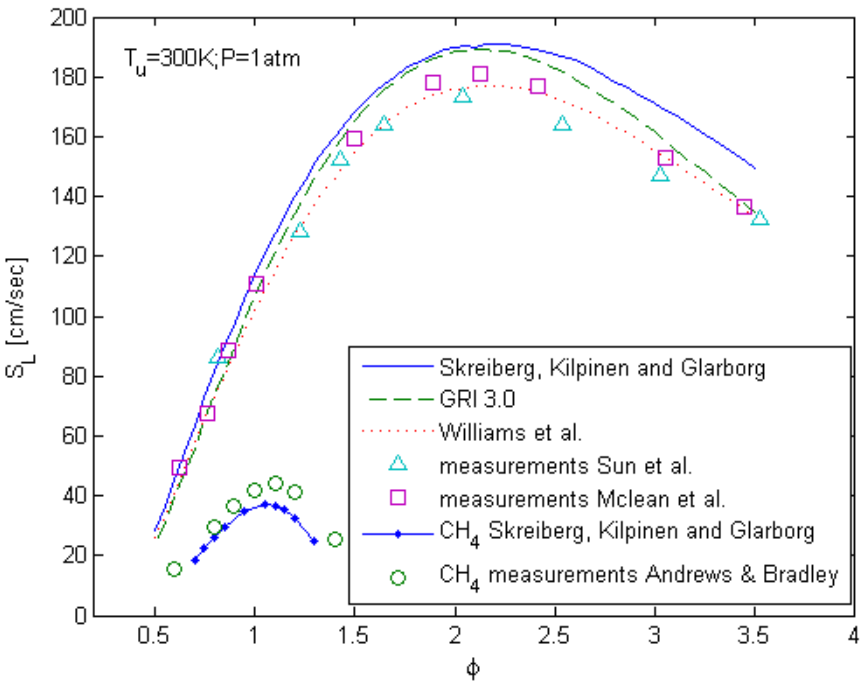

Figure 9. Laminar flame speeds for varying equivalence ratio of a 50:50 CO:H2 fuel mixture in atmospheric air at 300K. Comparison with methane. Key: Lines – simulations; symbols – measurements.

operational range of equivalence ratios around 0.5 the difference is only about a factor of 2. The point of stoichiometry has also changed from around $\phi = 1$ in the methane case to approximately $\phi = 2.3$ for the syngas case.

Figure 10 and Figure 11 shows the laminar flame speed versus equivalence ratio for 75:25 CO:H2 and 95:5 CO:H2 fuel mixtures at ambient conditions. In Figure 10 the trend for all mechanisms is the same; at lean equivalence ratios the discrepancies from experimental results are small. In Figure 11 the error increases with increasing

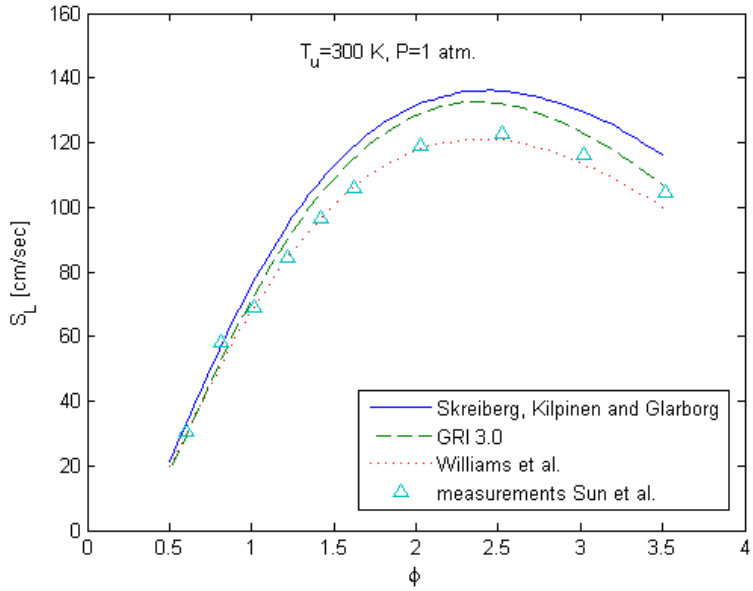

Figure 10. Laminar flame speeds for varying equivalence ratio of a 75:25 CO:H2 fuel mixture in atmospheric air at 300K, P=1atm. Key: Lines – simulations; symbols – measurements.

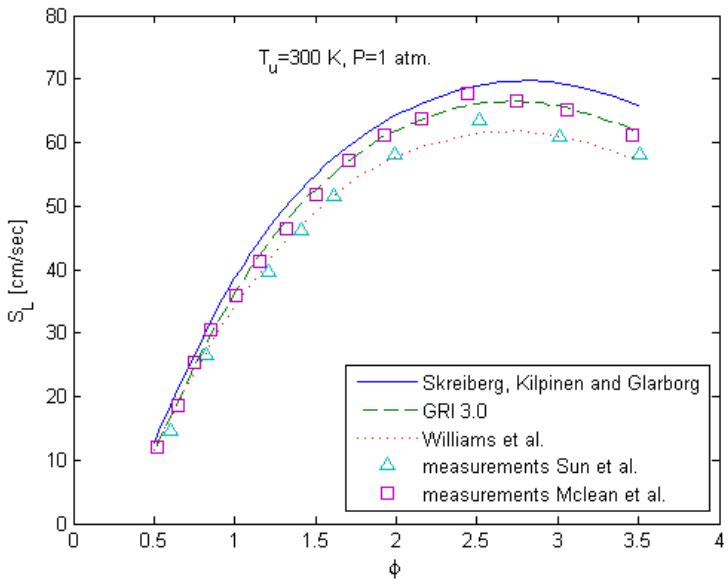

Figure 11. Laminar flame speeds for varying equivalence ratio of a 95:5 CO:H2 fuel mixture in atmospheric air at 300K. Key: Lines – simulations; symbols – measurements.

equivalence ratio for the Skreiberg et al case. Both the GRI-mechanism and the model of Williams et al show very good fit with the measurements of Mclean et al and Sun et al in Figure 11. The difference between the measured data sets is believed to be due to different measurements techniques and whether the flame stretch effect has been taken into account or not. The prediction of each mechanism depends on what experimental data set used in the optimization of that specific mechanism.

For lean conditions, that is of interest in gas turbine applications, Figure 12 clearly shows the dependence of the preheat temperature on the laminar flame speed. At low preheat temperature all the model predictions seems to agree quite well with experiments with the model by Skreiberg et al. being slightly over predicting. This discrepancy increases with increasing preheat temperature. The remaining model predictions seems to follow the experiments quite well until a preheat temperature of around 600 K is reached. For a preheat temperature of 700 K, a typical gas turbine preheat temperature, all the models over predict the measurements by at least 15-20 %.

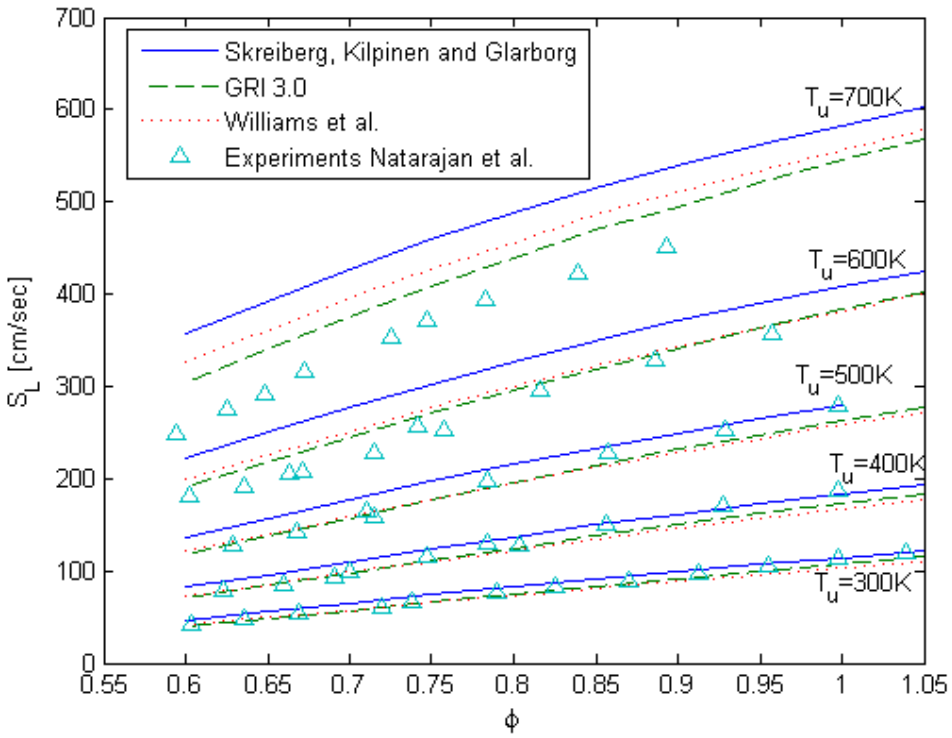

Figure 12. Laminar flame speed for a 50:50 H2:CO fuel mixture in air as a function of equivalence ratio for different preheat temperatures at 1 atm. Key: Lines – simulations; symbols – experiments.

The dependence of the laminar flame speed on equivalence ratio at elevated pressures is shown in Figure 13. Nitrogen in the air has been substituted for Helium to avoid flame wrinkling and instabilities that complicates the experimental data collection. Not completely representative of gas turbine running conditions this will at least be an approximation. The San Diego mechanism of Williams et al is the only one containing the Helium species and is therefore the only one included. The predictions for both pressure levels seem to agree well with the experimental data for lean equivalence ratios with the P=10 atm. case showing a slightly better fit for an equivalence ration below 2. For rich mixtures both predictions starts to diverge, the P=10 atm. case having the largest discrepancies around 20-30 %. Figure 14 shows the laminar flame speed as a function of equivalence ratio for a fuel mixture with high CO content at three different pressure levels. The model predictions of the mechanism by Williams et al show a good agreement with measurements for lean mixtures in similarity with previous results in Figure 13. The error increases with increasing equivalence ratio. Some minor discrepancies can be seen for the P=5 atm case at lean mixtures.

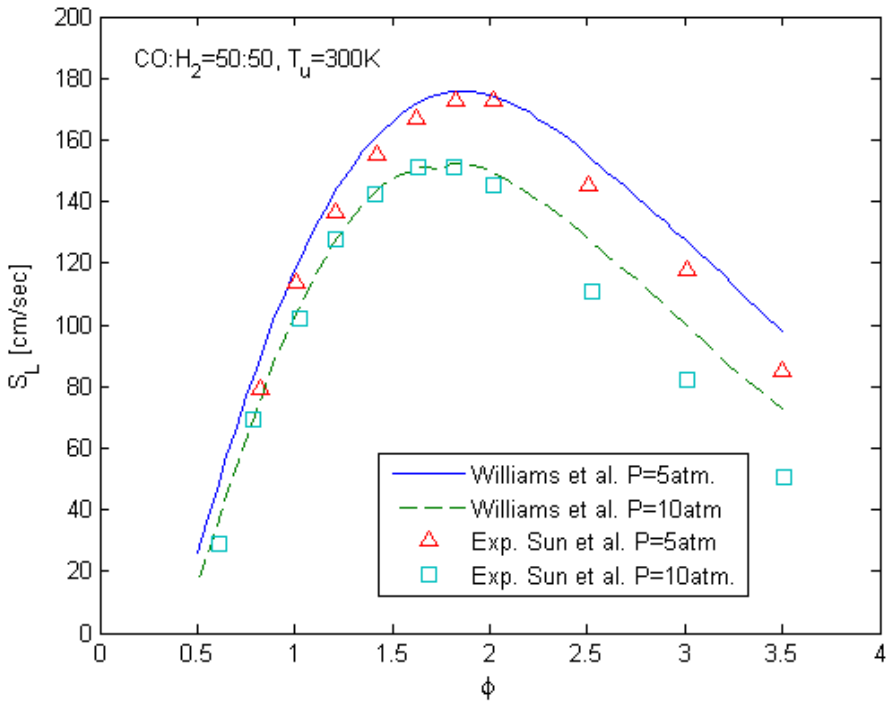

Figure 13. Laminar flame speed as a function of equivalence ratio for a 50:50 H2:CO fuel mixture (O2:He=1:7 oxidizer) at two different pressures; P=5atm and P=10atm. Preheat temperature Tu=300K. Key: Lines – predictions; symbols experiments.

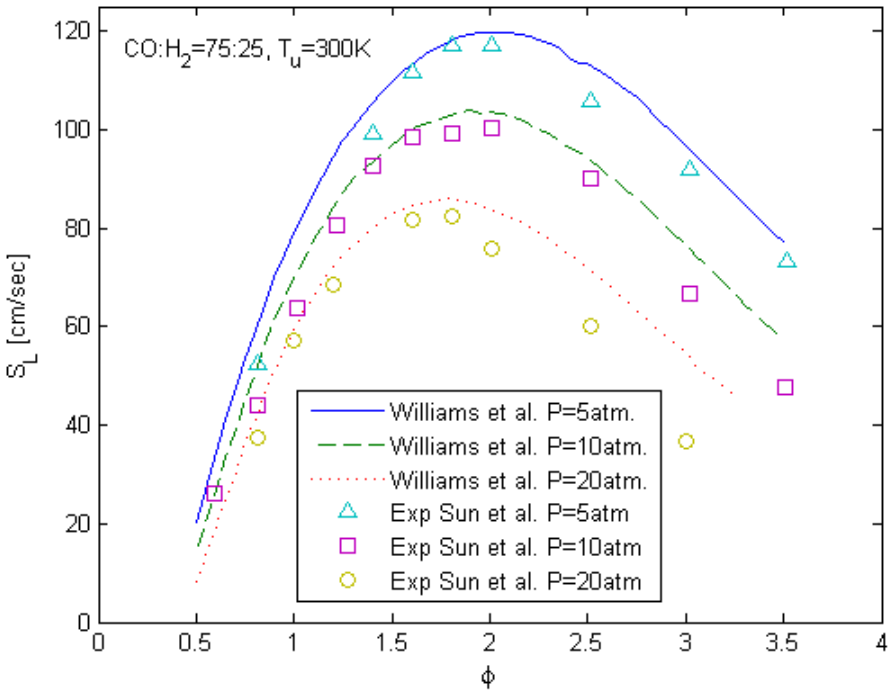

Figure 14. Laminar flame speed as a function of equivalence ratio for a 75:25 CO:H2 fuel mixture (O2:He=1:7 oxidizer) at three different pressures; P=5, 10, 20 atm. Preheat temperature Tu=300K. Key: Lines – predictions; symbols experiments.

Figure 15 shows the laminar flame speed as a function of equivalence ratio at elevated pressure and high preheat temperature. The oxidizer is in this case is also helium and oxygen due to the flame instability phenomena occurring at elevated pressures, hence only the mechanism of Williams et al. is included. The discrepancies between measurements and predictions are now smaller compared to atmospheric conditions at the same preheat temperature (see Figure 12).

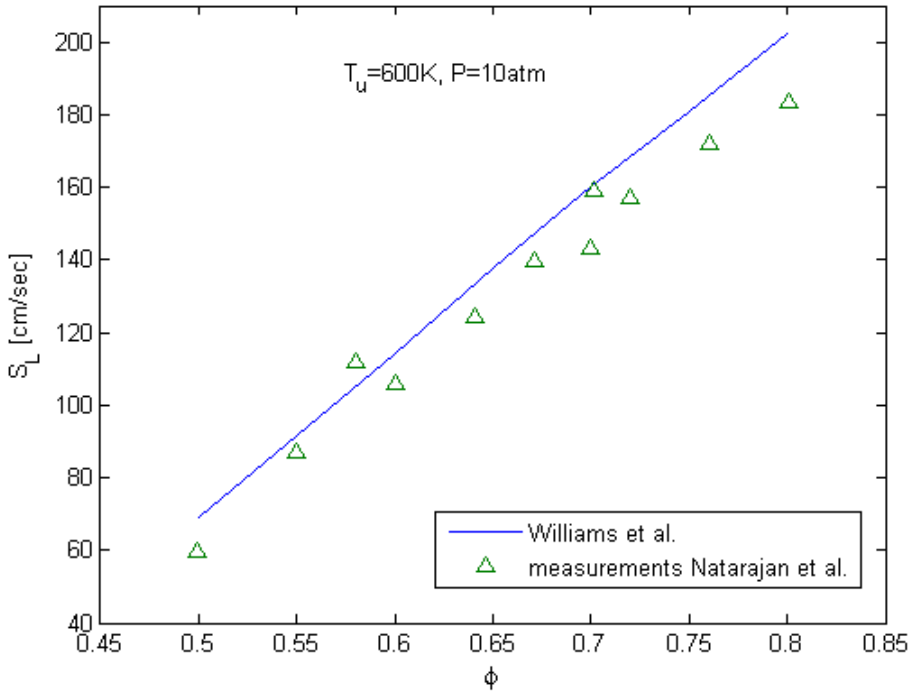

Figure 15. Laminar flame speeds for a 50:50 H2:C0 fuel mixture (O2:He=1:9 oxidizer) as a function of equivalence ratio at P=10atm and $T_u = 600K$. *Key: Lines – simulations; symbols – measurements.*

By fixing the equivalence ratio and preheat temperature the effect of the H2 content in the fuel can be seen as shown in Figure 16.
Following the results of Natarajan et al [17] the laminar flame speed increases with increasing H2 content in the fuel mixture due to the increases in thermal and mass diffusivity and the reaction rates The model prediction is slightly higher than the measurements and do not entirely follow the curvature from 30 % to 70 % H2, indicating that the sensitivity of the CO oxidation in the presence of H2 is not completely captured.

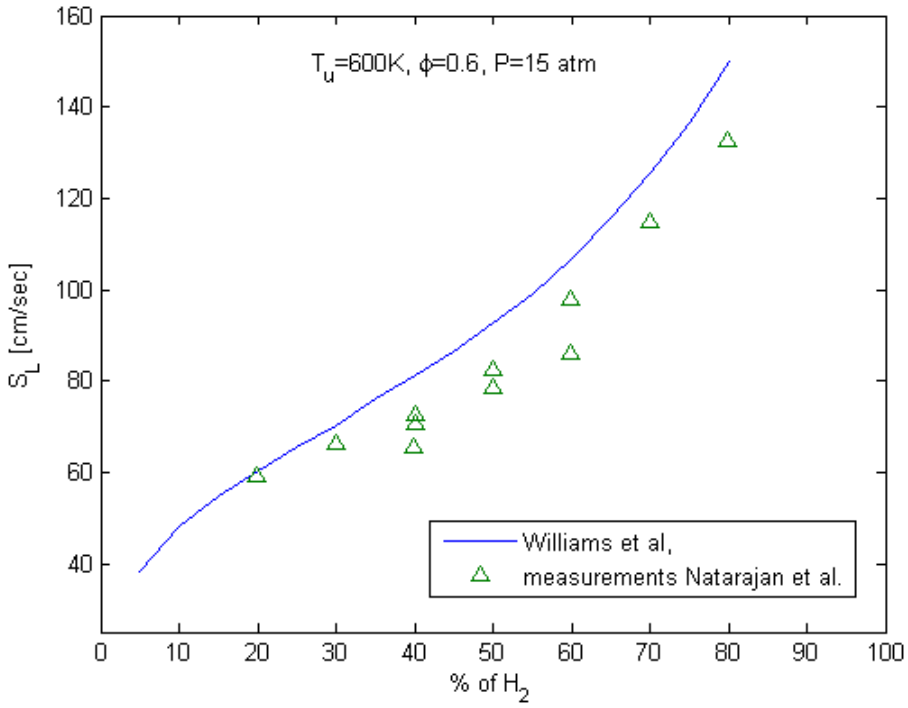

Figure 16. Laminar flame speed for different H2:CO fuel mixtures (O2:He 1:9 oxidizer) at a fixed equivalence ratio of 0.6, P=15atm and $T_u = 600K$. Key: Lines – simulations; symbols – measurements.

Figure 17 is a comparison of the solutions when using the approximate mixture-averaging of the transport properties versus using multi-component transport properties. The importance of multi-component transport becomes greater with increasing H2 content. The difference is very small for mixtures with a H2 concentration in the interval 0-50%. For high hydrogen content the effect of high mass diffusion becomes evident.
Here, the GRI 3.0 mechanism with air as an oxidizer has been used which creates convergence problems. Convergence could only be achieved by modifying the mesh, possibly introducing some errors in the converged solution.

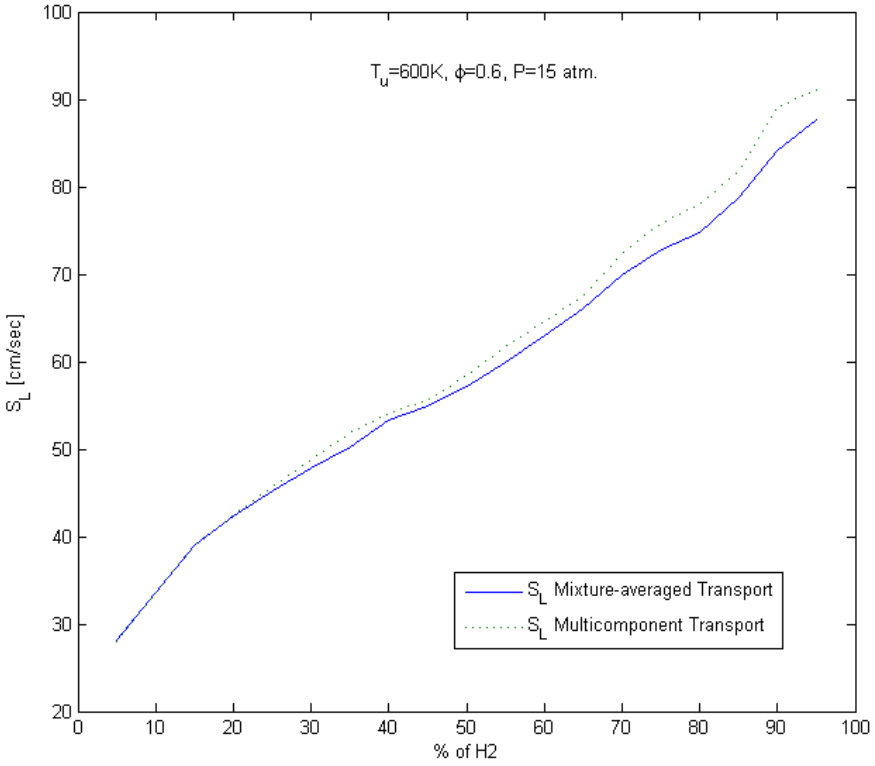

Figure 17. The dependence of H2 content on the laminar flame speed for a H2:CO fuel mixture at a preheat temperature of $T_u = 600K$ *equivalence ratio 0.6 and P=15 atm.*

Figure 18 shows the dependence of the ignition delay time on initial temperature on using a PFR model, the ignition delay time being defined by the maximum temperature gradient. All the models are slightly over predicting compared to measurements with an increasing error with increasing temperature. There is also a converging trend with increasing initial temperature for all the mechanisms. There is however a great difference in the results depending on the definition of the ignition time as can be seen when comparing Figure 18 and Figure 19.

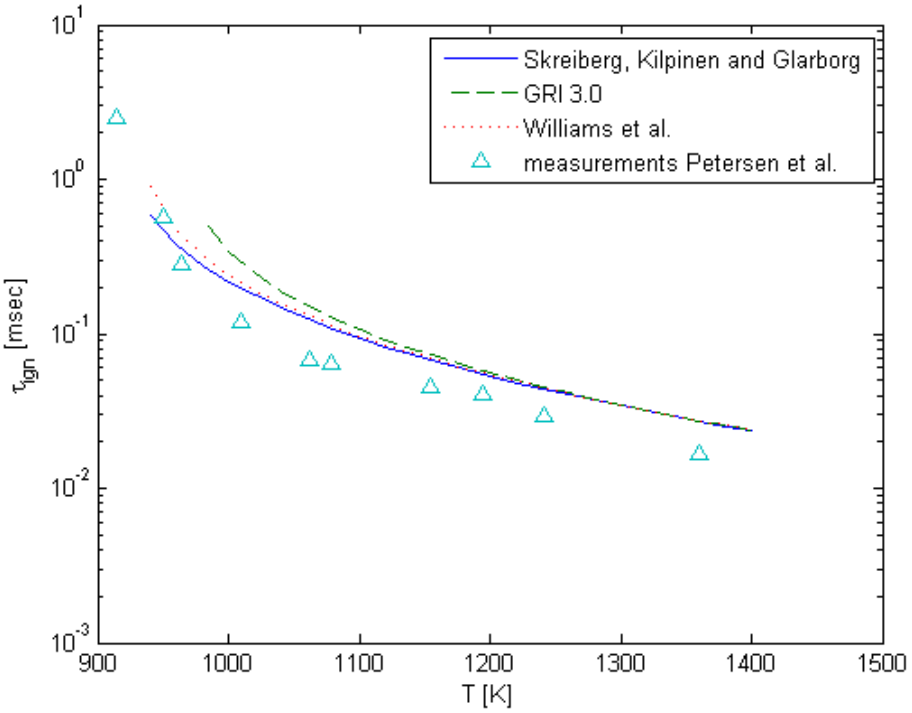

Figure 18. Ignition delay times as a function of initial temperature in a PFR for a 40:60 CO:H2 fuel mixture in air, P=1atm, equivalence ratio 0.5, Ignition time by max dT/dt. Key: Lines – simulations; symbols – measurements.

In Figure 19 all the models severely over-predict the ignition delay time compared to experimental data with the exception of very low initial temperatures. The great difference is explained by the definition of the ignition delay time used during the simulations and the method used in the experiments. The ignition delay times of Petersen et al. are based on the CH radical peak as opposed to OH- or HO2 peaks commonly used in ChemKin. The CH radical is not available in all the kinetic mechanisms used. Defining the ignition delay time by the maximum temperature gradient appears to produce reasonable accurate results.

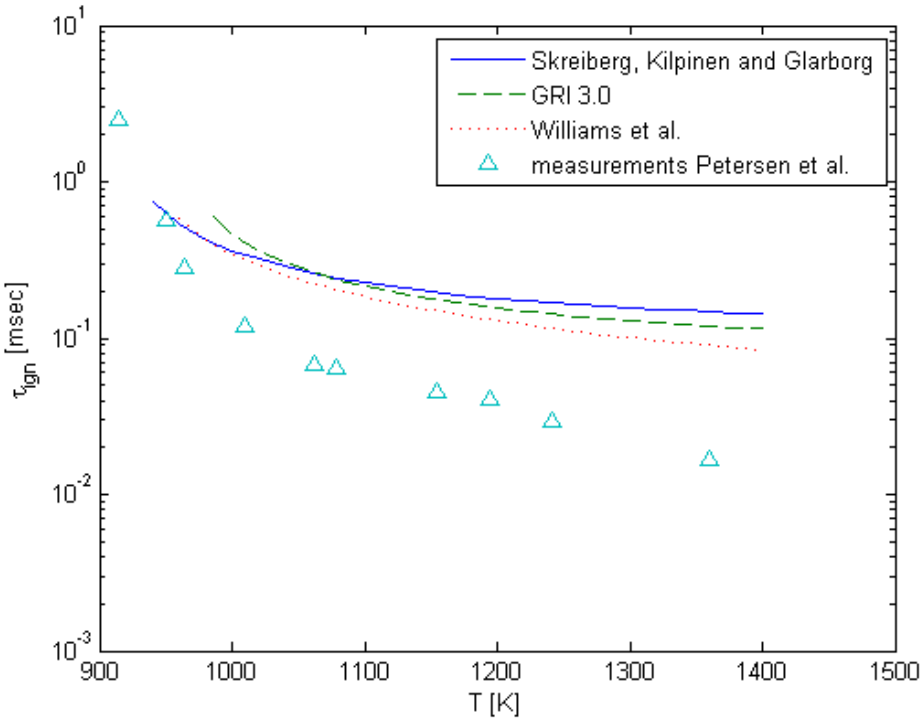

Figure 19. Ignition time delay as a function of initial temperature in a PFR for a 40:60 CO:H2 fuel mixture in air, P=1atm, equivalence ratio 0.5, Ignition time by d[OH]/dt=0. Key: Lines – simulations; symbols – measurements.

The temporal development of the temperature and the OH mole fraction in a PFR for a relatively low initial temperature of 940 K is shown in Figure 20. The maximum temperature derivative with respect to time occurs approximately at t=6.8 msec, whereas the OH radical peaks at approximately 11 msec (rel. error 38%).
For an initial temperature of 1400K (Figure 21) the maximum temperature gradient occurs approximately at t=0.02 msec and the OH radical mole fraction peaks at t=0.12msec (rel. error 83%) indicating a substantial difference in ignition delay time depending on in what way it is defined. The great difference in ignition delay could also be dependent on the numerical methods used to determine this local maximum.

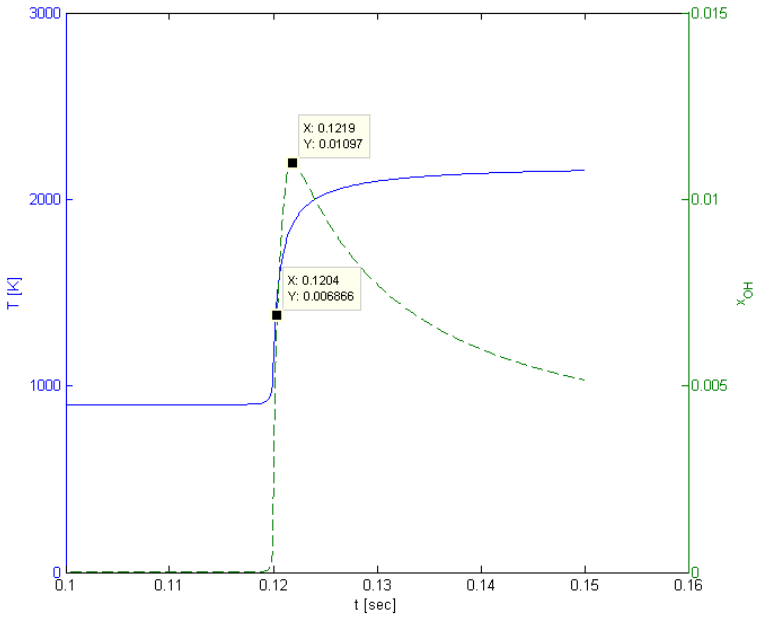

Figure 20. The temporal development of temperature and OH radical mole fraction in a PFR for a 40:60 CO:H2 fuel mixture in air at an initial temperature of 940 K, equivalence ratio 0.5, P=1atm using the mechanism of Skreiberg et al. Key: solid line – temperature; dashed line – OH mole fraction.

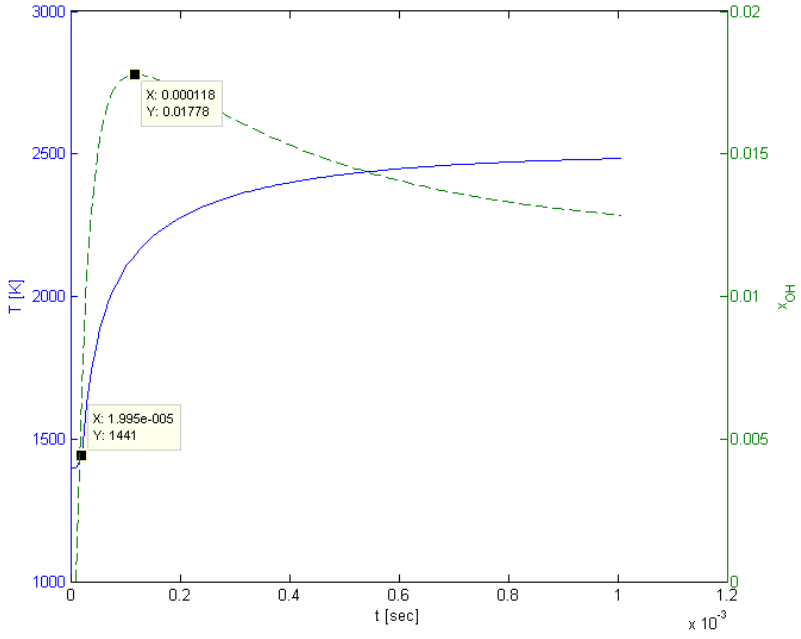

Figure 21. Temporal development of temperature and OH radical mole fraction in a PFR for a 40:60 CO:H2 fuel mixture in air at an initial temperature of 1400K, equivalence ratio 0.5, P=1atm using the mechanism of Skreiberg et al. Key: solid line – temperature; dashed line – OH mole fraction.

The temporal difference between HO2 peak and maximum temperature gradient (Figure 22) is much smaller indicating that the HO2 radical might better represent the actual ignition by rapid temperature increase.

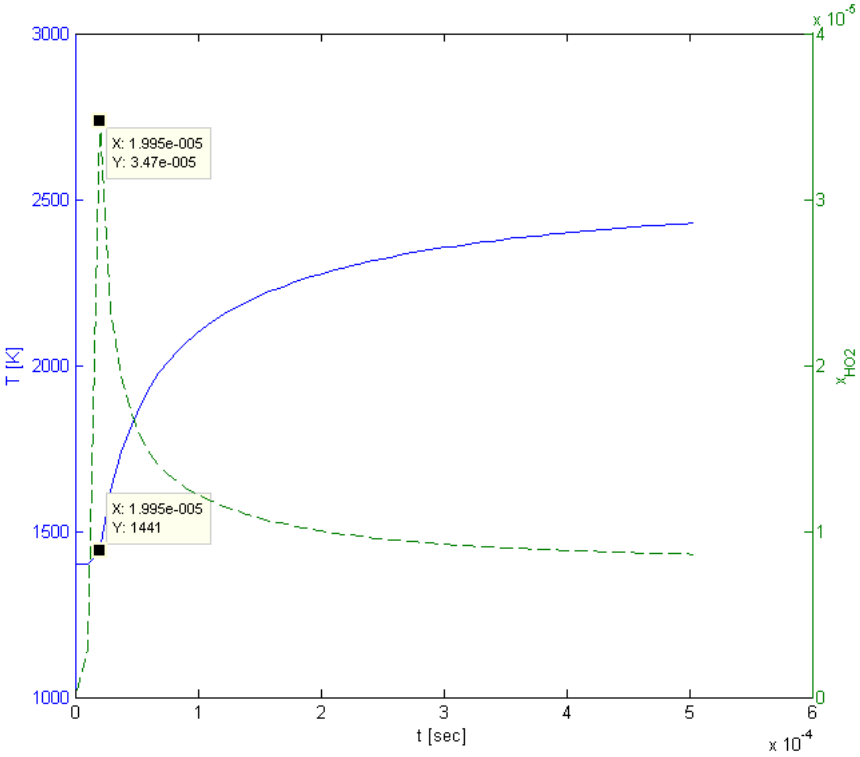

Figure 22. Temporal development of temperature and HO2 radical mole fraction in a PFR for a 40:60 CO:H2 fuel mixture in air at an initial temperature of 1400K, equivalence ratio 0.5, P=1atm using the mechanism of Skreiberg et al. Key: solid line – temperature; dashed line – HO2 mole fraction.

Figure 23 and Figure 24 shows the ignition delay as a function of initial temperature using a closed homogeneous constant pressure reactor determining the delay time by HO2 radical peaks and maximum temperature gradient respectively. The results are very similar for both methods but with some slight discrepancies for higher preheat temperatures.

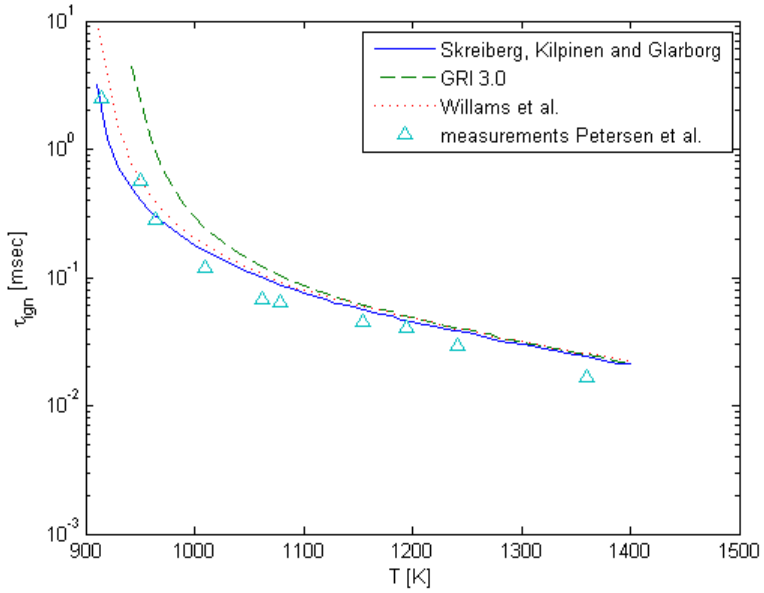

Figure 23. Ignition time delay as a function of initial temperature in a CHR for a 40:60 CO:H2 fuel mixture in air, P=1atm, equivalence ratio 0.5, Ignition time by d[HO2]/dt=0. Key: Lines – simulations; symbols – measurements.

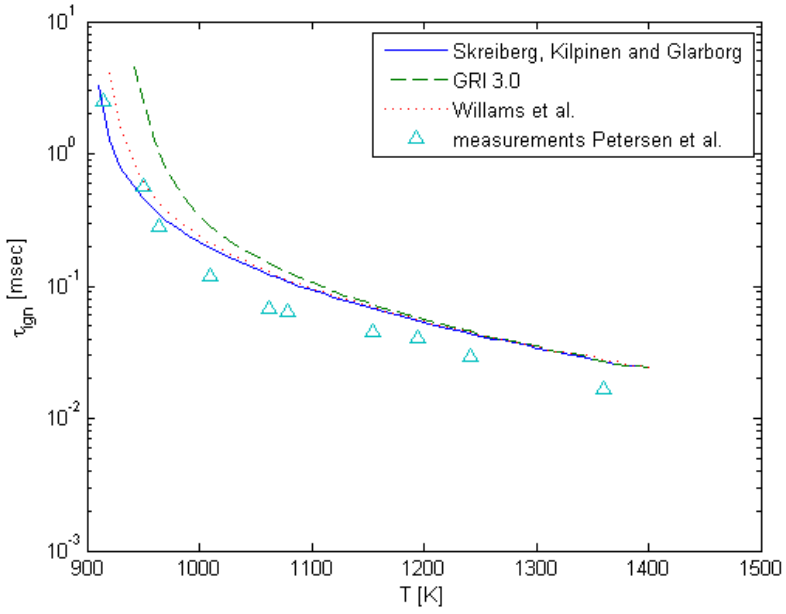

Figure 24. Ignition time delay as a function of initial temperature in a CHR for a 40:60 CO:H2 fuel mixture in air, P=1atm, equivalence ratio 0.5, Ignition time by max dT/dt. Key: Lines – simulations; symbols – measurements.

The effect of elevated pressure on the ignition delay is shown in Figure 25 and Figure 26. The GRI 3.0 mechanism under predicts the ignition delay time for both P=20 atm. and P=23 atm. For both pressures the model of Skreiberg et al. seems to agree the best with the experimental data being slightly over-predicting at lower initial temperatures.
The model of Williams et al. has quite a good agreement for P=23 atm. The discrepancies between the models seem to increase with decreasing initial temperature which might indicate differences in the key rate parameters controlling ignition. The differences decrease with increasing initial temperature as gas turbine like conditions are approached.
The effect on ignition time by the definition; OH peak versus maximum temperature gradient seems to vanish at elevated pressures. Figure 25 and Figure 26 are practically identical.
Replacing carbon monoxide with methane could also have an effect on the reaction pathways affecting the development of the OH radical, thus making the OH concentration coincide better with the development of the temperature.

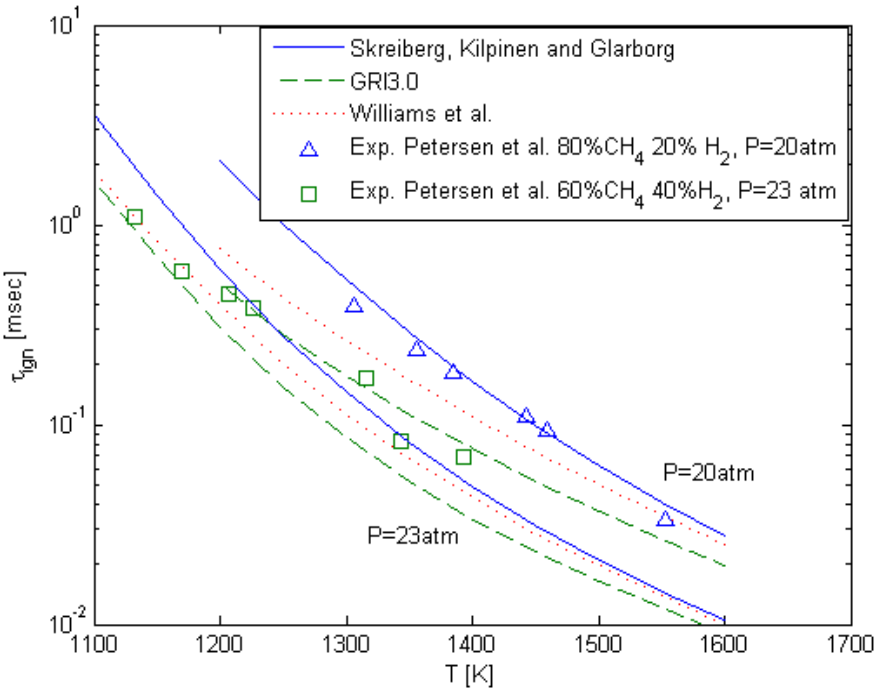

Figure 25. Ignition delay time as a function of temperature in a PFR for 80:20 CH4:H2 and 60:40 CH4:H2 fuel mixtures in air at pressures P=20atm and P=23atm and an equivalence ratio of 0.5. Ignition time by d[OH]/dt=0 Key: Lines – simulations; symbols – measurements.

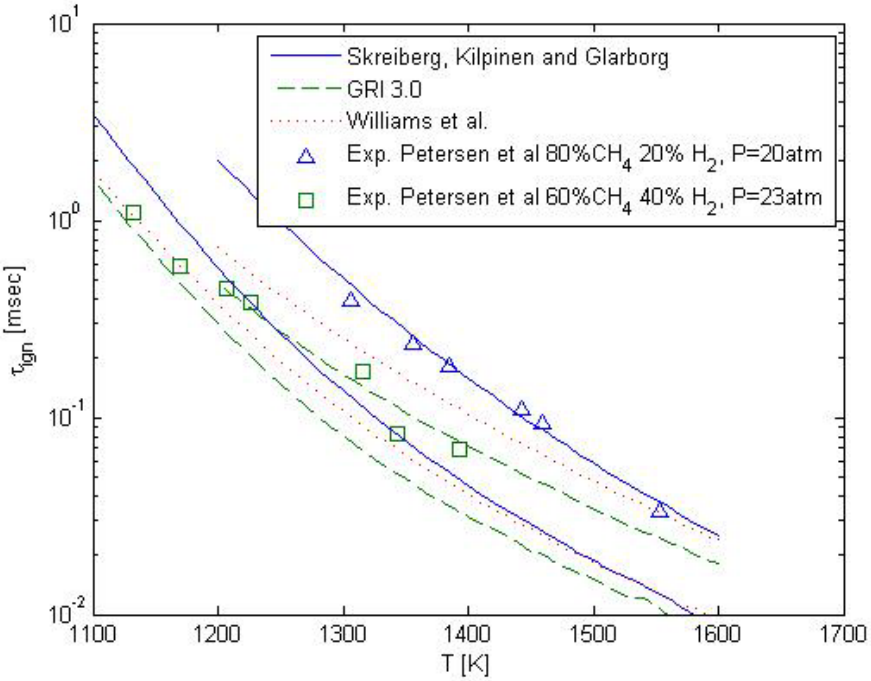

Figure 26. Ignition delay time as a function of temperature in a PFR for 80:20 CH4:H2 and 60:40 CH4:H2 fuel mixtures in air at pressures P=20atm and P=23atm and an equivalence ratio of 0.5. Ignition time by max dT/dt Key: Lines – simulations; symbols – measurements.

5.5.2 Cantera Simulations

Laminar flame speed predictions were also obtained from the Cantera code to test its performance. Below are some test cases reproduced and compared to the results of ChemKin and experimental data.

By examining Figure 27 and Figure 28 it becomes clear that there are substantial differences between the numerical predictions obtained from ChemKin and Cantera. The results from Cantera are overall 10-15 % higher than the predictions of ChemKin. The influence of mixture composition seems to have a negligible effect and the trend of the different mechanisms seems to be the same. Figure 29 shows a close up view of the predictions close to maximum flame speed where the instability of the Cantera solver can be seen more clearly as irregularities in the curves. Appendix A shows the corresponding laminar flame speed predictions of Cantera with experimental data for the 50:50 and 75:25 CO:H2 mixture.

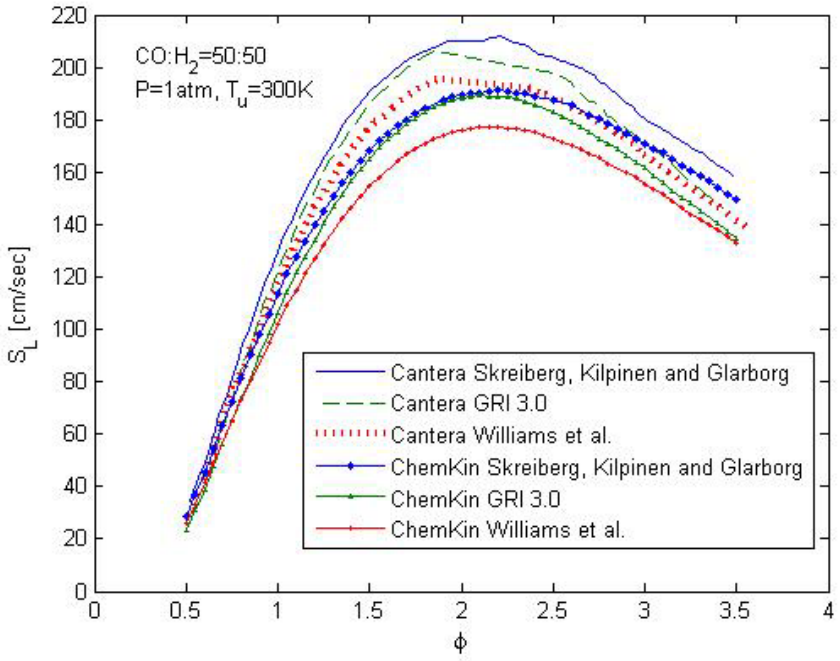

Figure 27. Comparison of Laminar flame speeds for varying equivalence ratio of a 50:50 CO:H2 fuel mixture in atmospheric air at 300K, P=1atm. Key: Solid Lines – Cantera predictions; Lines with symbols – ChemKin predictions.

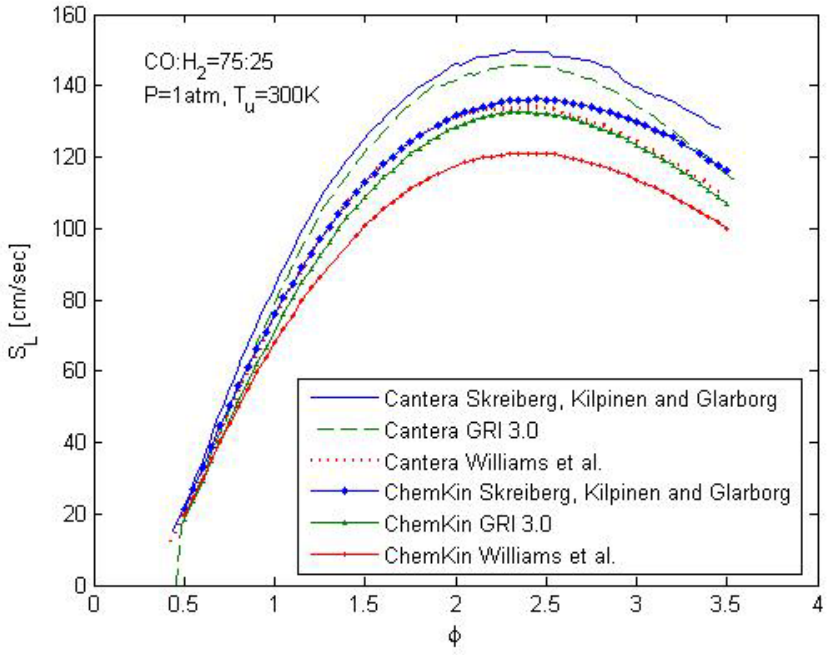

Figure 28. Comparison of Laminar flame speeds for varying equivalence ratio of a 75:25 CO:H2 fuel mixture in atmospheric air at 300K, P=1atm. Key: Solid Lines – Cantera predictions; Lines with symbols – ChemKin predictions.

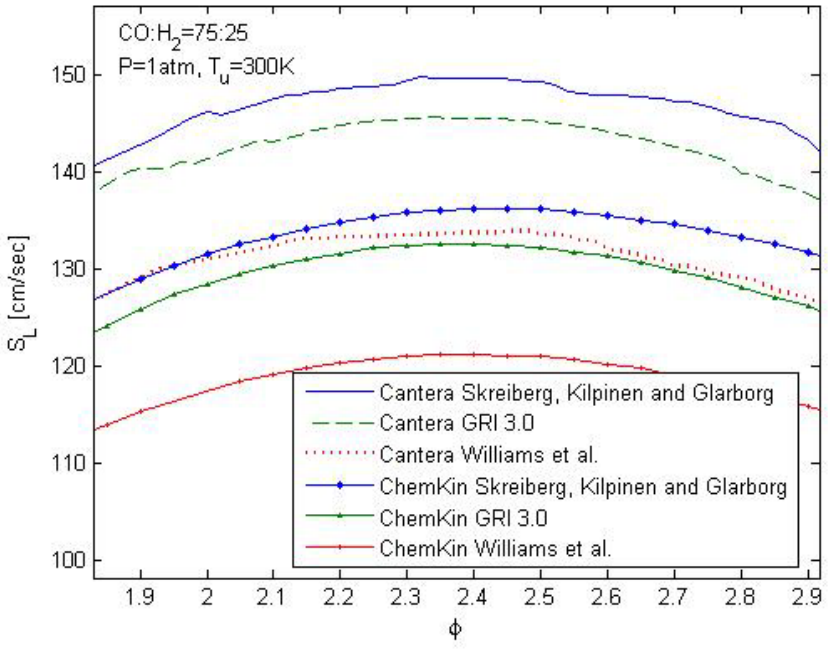

Figure 29. A close-up comparison of Laminar flame speeds for varying equivalence ratio of a 75:25 CO:H2 fuel mixture in atmospheric air at 300K, P=1atm. Key: Solid Lines – Cantera predictions; Lines with symbols – ChemKin predictions.

Figure 30 show the laminar flame speed predictions of Cantera for varying equivalence ratio at different preheat temperatures. At low preheat temperatures all the mechanisms over predict the laminar flame speed compared to measured data. With increasing preheat temperature the discrepancies grow very large. The relative error at a preheat temperature of 700 K is about 40 % for the mechanism of Skreiberg et al. At 500 K preheat temperature a diverging trend can be seen for increasing equivalence ratio.

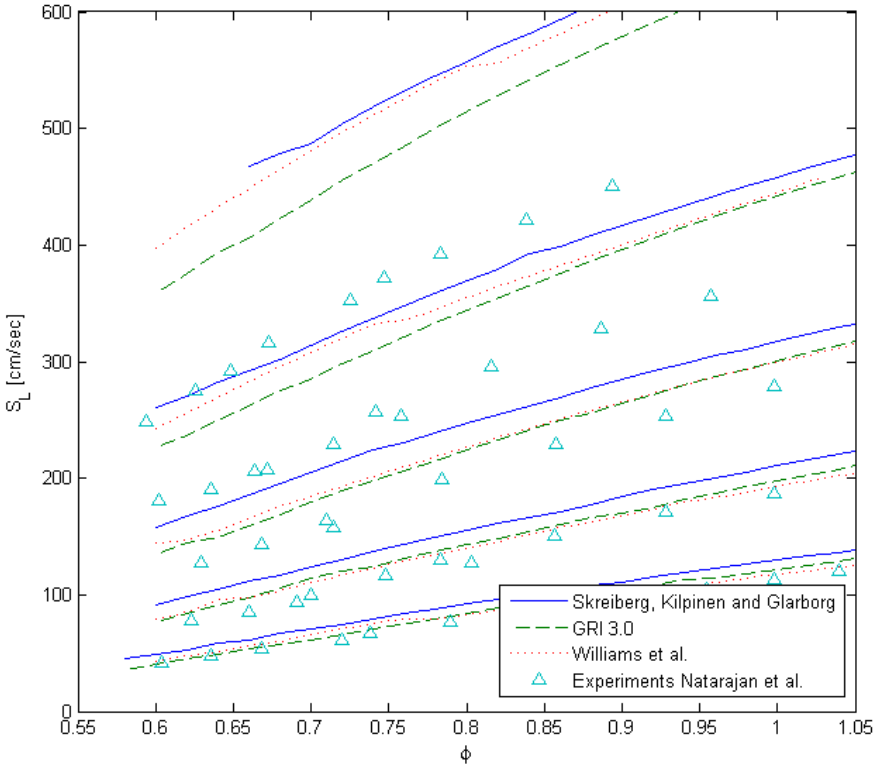

Figure 30. Laminar flame speed for a 50:50 H2:CO fuel mixture in air as a function of equivalence ratio for different preheat temperatures at 1 atm. Key: Lines – simulations; symbols – experiments.

A detailed comparison of the predictions of Cantera and ChemKin at high temperature can be seen in Figure 31. The Cantera results for a H2:CO 50:50 mixture in air over predict the measured data even more than the predictions of ChemKin. Also note the unstable behavior of the Cantera prediction.

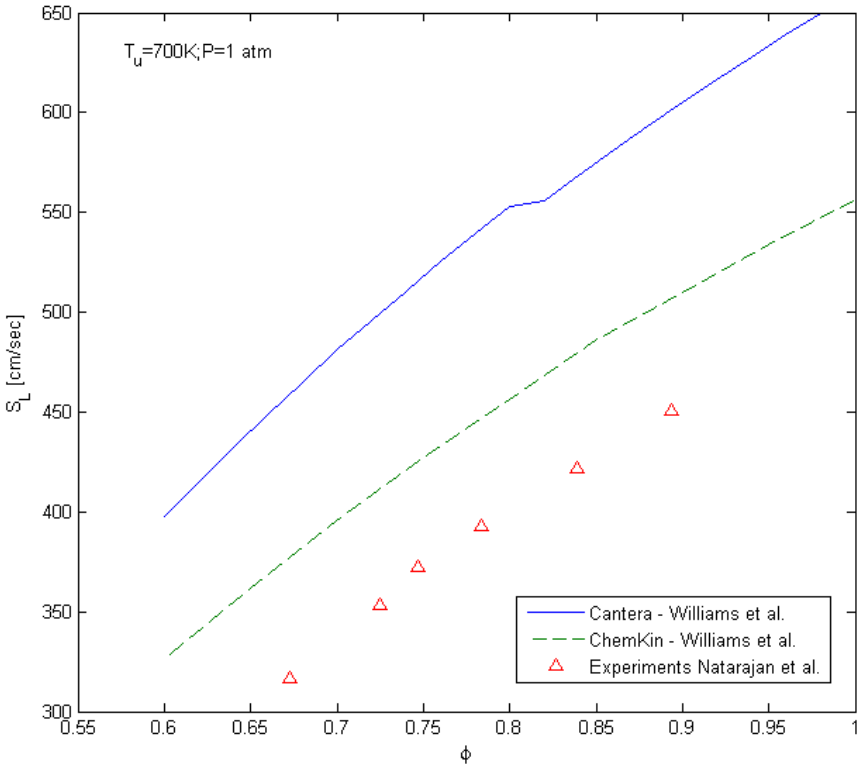

Figure 31. Comparison of predicted laminar flame speeds produced by Cantera and ChemKin for a 50:50 H2:CO mixture in air with varying equivalence ratio at a preheat temperature of 700K, P=1atm. Key: Lines – simulations; symbols – experiments.

Figure 32 shows a comparison of the predicted laminar flame speeds produced by Cantera and Chemkin at elevated pressures. The mechanism used is the one of Williams et al. Discrepancies can be seen between the two solutions. Cantera is consistently over predicting the laminar flame speed compared to ChemKin results and measurements at equivalence ratios close to stoichiometry and on the rich side. The error however seems to be smaller at elevated pressures than atmospheric. The instabilities and fluctuations of the converged Cantera solution is however still present.

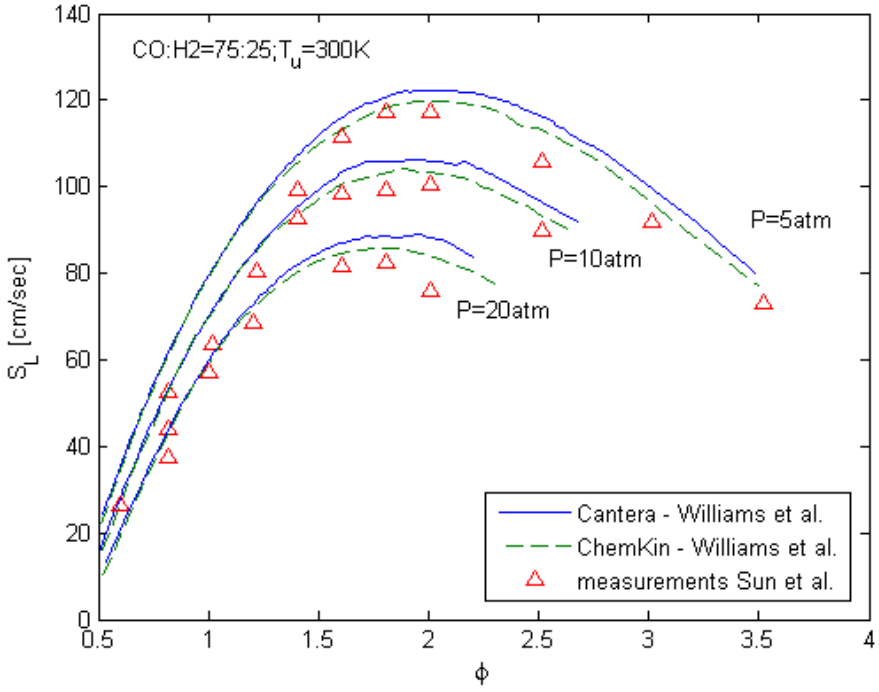

Figure 32. Comparison of Laminar Flame Speed predictions of Cantera and ChemKin for a 75:25 CO:H2 fuel mixture (O2:He=1:7 oxidizer) for varying equivalence ratio at three different pressures. Key: Lines – predictions: symbols – experiments.

A closed homogeneous constant pressure reactor model was also run in Cantera and the results using maximum temperature gradients to define ignition temperature are practically identical to the ChemKin predictions as shown in Figure 33.

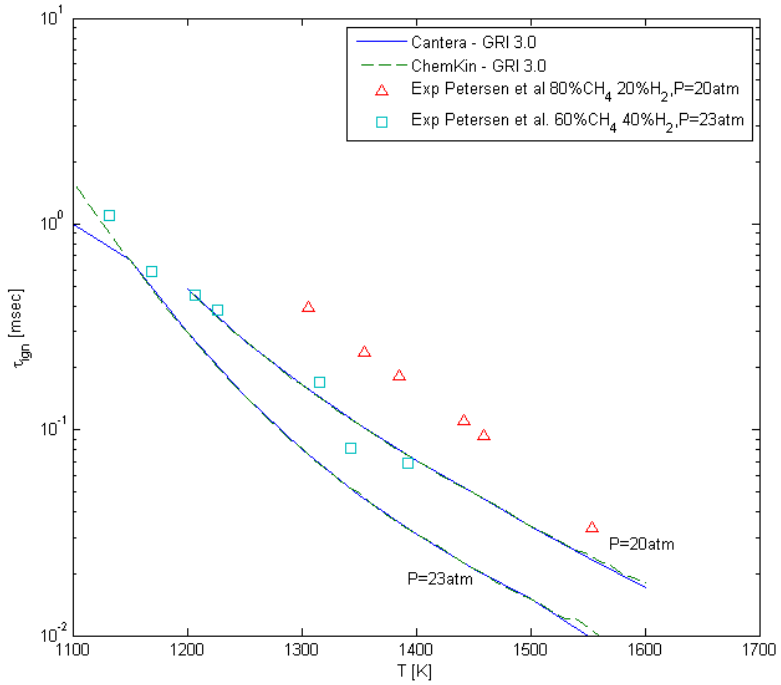

Figure 33. Ignition delay time as a function of temperature in a CHR for 80:20 CH4:H2 and 60:40 CH4:H2 fuel mixtures in air at pressures P=20atm and P=23atm and an equivalence ratio of 0.5. Ignition time by max dT/dt Key: Lines – predictions of Cantera and ChemKin using the mechanism of Williams et al; symbols – measurements.

5.6 Conclusions & Discussion

5.6.1 Mechanism selection - ChemKin

Below are the absolute relative errors between predictions and experimental data at maximum laminar flame speed summarized with the absolute relative error calculated as

$$\left| \frac{S_{L,\max,} - S_{L,\max,experimental}}{S_{L,\max}} \right| \tag{68}$$

For the high temperature predictions, the value at the lowest equivalence ratio was used. Table 3 show a summary of the absolute relative errors against experimental data of the maximum value of the laminar flame speed predictions by ChemKin, the largest errors in bold.

Table 3 Relative error of ChemKin maximum laminar flame speed predictions against experiments

P [atm]		1				5	
Tu [K]		300			700	300	
Mechanism	CO:H2	50:50	75:25	95:5	50:50	50:50	75:25
Skreiberg et al		**7%**	**11%**	**9%**	**29%**	-	-
GRI 3.0		5%	2%	4%	17%	-	-
Williams et al.		1%	<1%	3%	23%	<1%	2%
P [atm]		10			20		
Tu [K]		300		600	300		
Mechanism	CO:H2	50:50	75:25	50:50	75:25		
Skreiberg et al		-	-	-	-		
GRI 3.0		-	-	-	-		
Williams et al.		<1%	3%	10%	2%		

Table 4 displays a summary of the absolute relative error between ignition delay predictions by ChemKin and experimental data at a fixed initial temperature T=1200K.

Table 4 Relative error of ChemKin ignition delay predictions against experiments at T=1200K

P [atm]	1			
Mixture	CO:H2 40:60			
Reactor	PFR		CHR	
Mechanism	dT/dt	d[OH]/dt	dT/dt	d[HO2]/dt
Skreiberg et al	50%	**78%**	19%	11%
GRI 3.0	**55%**	73%	**20%**	**12%**
Williams et al.	50%	63%	19%	11%
P [atm]	20		23	
Mixture	CH4:H2 80:20		CH4:H2 60:40	
Reactor	PFR		PFR	
Mechanism	dT/dt	d[OH]/dt	dT/dt	d[OH]/dt
Skreiberg et al	50%	50%	25%	25%
GRI 3.0	**120%**	**100%**	**50%**	**50%**
Williams et al.	43%	43%	29%	12%

All the mechanisms predict laminar flame speed quite well for binary lean mixtures of hydrogen and carbon monoxide. A general trend of increasing error against measurements for increasing equivalence ratio is also clear, where the mechanism of Skreiberg et al is the most over-predicting. The mechanism of Williams et al has the best fit to experimental data according to the tables 3 and 4.
With increasing preheat temperature the discrepancies to measurements increase severely. At gas turbine-like conditions of preheat temperatures around 600-700K the error is substantial; 29% for Skreiberg et al and 23% for Williams et al at 700K. This might indicate an inaccurate temperature dependence of the reaction rates.

The discrepancies in the experimental flame speed data used for validation might be explained by the measurement technique used and if the flame stretch effect has been taken into account or not. This also includes an uncertainty in the choice of kinetic mechanism.

Of the three mechanisms tested the most suitable mechanism for laminar flame speed predictions for syngas at atmospheric conditions is the one by Williams et al.

Laminar flame speed data of syngas-like mixtures also containing methane that would better represent gas turbine conditions is not available; hence the possible interaction of adding methane and higher order hydrocarbons representing natural gas is not covered.

For ignition delay time predictions of a plug-flow reactor and a closed homogeneous constant pressure reactor are quite similar at atmospheric conditions. The key differences lie in the definition of ignition. The use of the point with the maximum temperature gradient seems to be the most physically reasonable definition. The HO2 radical concentration peak seems closely related to the overall temperature increase whereas the OH radical concentration might have several local maxima at certain conditions.

At elevated pressures the only experimental flame speed data available has been obtained using oxygen and helium as an 'artificial' atmosphere. This limits the test to the Williams mechanism only since this is the only mechanism containing Helium as a species. The overall trend at elevated pressures is similar to the atmospheric one; for lean mixtures the agreement is quite good with increasing error for increasing equivalence ratio. At high preheat temperatures, lean mixtures the large error occurring at atmospheric conditions is somewhat reduced when running at high pressure. Multi-component transport properties become increasingly important as the amount of light highly diffusive species is increased. Mixture-averaged transport properties can be used with a relative error less than 2 % for fuel mixtures with hydrogen content below 50 % by volume for that specific syngas fuel mixture.

For ignition delay time predictions at elevated pressure the mechanism of Skreiberg et al gives the best performance, whereas the GRI3.0-mechanism clearly under predict the ignition delay time for binary methane-hydrogen mixtures.

The overall conclusion is that none of the mechanisms tested are really suitable for predicting laminar flame speeds of pure syngas mixtures. However, for the purpose of co-firing with natural gas which is of main interest here; the mechanism of Williams et al is considered to produce adequate results for ignition delay and laminar flame speed predictions.

5.6.2 Cantera performance

Table 5 show a summary of the absolute relative error between laminar flame speed predictions by Cantera and experiments.

Table 5 Relative error of Cantera maximum laminar flame speed predictions against experiments.

P [atm]		1				5	
Tu [K]		300			700	300	
Mechanism	CO:H2	50:50	75:25	95:5	50:50	50:50	75:25
Skreiberg et al		**17%**	**18%**	-	**42%**	-	-
GRI 3.0		13%	16%	-	30%	-	-
Williams et al.		11%	10%	-	38%	-	3%
P [atm]		10			20		
Tu [K]		300		600	300		
Mechanism	CO:H2	50:50	75:25	50:50	75:25		
Skreiberg et al		-	-	-	-		
GRI 3.0		-	-	-	-		
Williams et al.		-	7%	-	6%		

The major difference between the PREMIX code of ChemKin and the Cantera code is a consistent substantial over-prediction of laminar flame speed by Cantera at atmospheric conditions. The reason for this is not clear. It is possible that differences in the discretization schemes might cause some errors. Using slightly different grid refinement parameters might also affect the final solution. Especially in stoichiometric mixtures where the flame speed is high and solution gradients are steep. It also seems like that the key parameter affecting the robustness of the Cantera solver is temperature, or indirectly the equivalence ratio. At certain equivalence ratios (corresponding to a temperature) convergence problems arise. Increasing the preheat temperature also affects the total error of the converged solution. A detailed investigation of this is however considered to be outside the scope of this thesis.

The large differences between predictions of ChemKin and Cantera decrease as the pressure is increased. Increased pressure affect the reaction zone, in other words the gradients steepen even further. With less strict grid refinement parameters in the Cantera simulations, steeper gradients by increases in pressure might reduce the error for stoichiometric mixtures.
The closed homogeneous constant-pressure reactors of ChemKin and Cantera provide almost identical results for ignition delay time predictions.

ChemKin would be the preferred software to use in future work when usability in terms of quick problem setup is taken into account, whereas Cantera might be more flexible but requires more programming skills and numerical troubleshooting.

6 Investigations of the Global Chemical Time Scale

6.1 Introduction

This section describes the numerical investigation of the dependence of the global chemical time scale on various mixtures and initial conditions. An attempt to characterize the burner stability using the global chemical time scale is also treated here.

6.2 Rig Test Data

The simulations are based on the experimental data obtained and observations made during single burner rig tests conducted at Siemens in Finspong SE and Lincoln UK. The tests were performed by running the single burner with different fuel mixtures and observing the behaviour of the flame, performing measurements of NOx and CO emissions and burner pressure drop. Both 'binary' mixtures of natural gas and one single added component as well as multi-component fuel mixtures were tested. Only two-component mixtures were however considered in this study. The range of fuel mixtures used is listed below.

Table 6 Fuel mixtures used in the simulations with corresponding Wobbe Index range

Gas Mixture	WI (MJ/m3)
Natural Gas-N2	48-0
Natural Gas-CO2	48-0
Natural Gas-CO	48-12
Natural Gas-H2	48-39
Natural Gas-CO-H2	48-12

The tests were performed with an unmodified standard LB000 reference burner originally built for the SGT-700. The experimental data points were selected for this study based on the following requirements:

- No pilot fuel flow, hence full premix considered only.
- No central gas flow to ensure mixture homogeneity.

To assure maximum homogeneity of the fuel mixture data points with central gas or pilot fuel flow were not considered.

6.3 Standard Natural Gas Approximation

In the calculations the composition of natural gas has been approximated with the fuel components displayed in the table below. All higher hydrocarbons >C3 (>propane C3H8) have been approximated as propane since the mechanism used only includes hydrocarbons up to C3. Any effects of the higher order hydrocarbons on the reaction pathways are neglected. A comparison of the laminar flame speed of pure methane and the standard natural gas approximation above is presented in appendix B. The maximum

relative difference of 15% occurs close to stoichiometric. Approximating standard natural gas with pure methane is therefore not physically reasonable.

Table 7 Standard natural gas composition used in the simulations.

Gas Specification Monthly average Swedegas March-September 2007			
Component			Avg
Methane	CH4		89.55%
Ethane	C2H6		5.95%
>Propane	>C3H8		4.50%

6.4 Numerical Method

The numerical simulations were all based on the parameter ranges used in the rig tests. From these parameter sets laminar flame speeds were simulated with additional processing of the solution data to obtain flame thickness and global chemical time estimates according to the theory in section 4.
For simulating laminar flame speeds the PREMIX code in the ChemKin package was used in the same manner as in previous chapters (5.4.3), although both multi-component transport properties and effects of thermal diffusion were included. Using multi-component transport properties is recommended for multi-component fuel mixtures to provide enough accuracy. The solutions were then post-processed in a custom Matlab script to calculate time scales and for visualization of results. Pressure and preheat temperature were set according to the rig test conditions.

6.5 Influence of mixture composition

To isolate the effect of mixture composition on the laminar chemical time scale, flame speed simulations were performed at various fixed flame temperatures. In varying the mixture composition the equivalence ratio was adjusted accordingly to maintain a constant flame temperature. In this way the temperature effect on the flame speed was removed. Relevant physical parameters used are presented in Table 8.

Table 8 Physical simulation parameters used for the fixed flame temperature simulations

Parameter	Value
Pressure (bar)	16
Preheat Temperature Tu (K)	693
Flame Temperatures (K)	1650-1850

Further, investigations of the dependence of mixture composition and equivalence ratio on the chemical time scale were conducted along with diagrams showing the flame temperature as a function of mixture composition and equivalence ratio to use for comparisons.
Various attempts to correlate the global laminar chemical time scale with mixture composition at flameout and flameback were made. Following the theory of chapter 3 it is clear that the turbulent time scales at flameout have to be approximated from experiments and or Computational Fluid Dynamics to be able to determine the flameout

and flashback limits. To be able to represent the experimental data in these investigations, average mixture equivalence ratios were calculated from the measured air and fuel mass flows.
The theory of chapter 3 further states that the fluid dynamic properties must not change to any greater extent. The mean and RMS-values of inlet temperature and mass flow of the selected data varies less than 0.5% making this a fulfilled condition. The exact sensitivity of mass flow perturbations in the entire system is however not known. Therefore comparisons with the experimental data were made internally to if possible, find an approximate trend of the flameout and flashback limit. The amount of data for the syngas – natural gas mixtures (bottom row of Table 6) was insufficient for use in the calculations. A mixture of 50:50 H2:CO syngas mixed into natural gas was simulated at 18 bar pressure to find possible interactions between hydrogen and carbon monoxide as well as any effects of pressure on the chemical time scale. Some 1600 simulations were performed for the mappings.
For very low equivalence ratios close to the lean flammability limit the convergence of ChemKin proved to be very poor at some times. Linear interpolation was used to approximate some of these points to be able to produce a contour plot. This approximation will have to be considered sufficient in the case of mapping the gas kinetic behavior.

Table 9 Physical simulation parameters used for flameback/flameout mappings

Parameter	Value
Pressure (bar)	1, 16 and18
Preheat Temperature Tu (K)	693
Equivalence ratio	0.30-1.0
Fraction of added fuel	0-100%

7 Ignition Delay

Further guided by chapter 3 it is clear that for an arbitrary combustor the dependence of mixture composition and equivalence ratio on the auto ignition delay is of interest. Ignition delay calculations were performed using a closed homogeneous constant pressure reactor *(CHR)* to map the behavior of the ignition delay time scale, i.e. the reactant mixture is assumed to be homogeneous (infinitely fast mixing in the mixing tube) and the heat transfer from the tube wall is infinitely fast.

From the conclusions of chapter 5 the maximum temperature gradient was used to define the point of ignition of the fuel mixture. Similar as in the previous chapter the mechanism of Williams et al was used to model the formation and consumption of chemical species. In chapter 6 the physical parameters were chosen according to the available rig test data. Under those conditions, both atmospheric and elevated pressure, the preheat temperature is too low to initiate auto ignition; hence a direct comparison between the two time scales at those conditions is not possible.

The ignition temperature of natural gas alone at atmospheric pressure is around 773K and for hydrogen 793K. The temperature for auto ignition decreases with increased pressure.

By selecting a sufficiently high preheat temperature, auto ignition for 100% NG can be assured with an ignition delay on the order of 3 msec and the behavior with respect to mixture composition and equivalence ratio can be visualized. The determination of the appropriate preheat temperature was based on the approximate critical flow residence time $\tau_{ig} = t_{c,3}$ for a pure natural gas mixture. Further details can be found in appendix 0.

Calculations of ignition delay time were also performed at lower preheat temperatures for comparisons. The relevant physical parameters for the simulations are summarized below. Some 2000 simulations were performed.

Table 10 Relevant physical parameters for ignition delay simulations

Parameter	Value
Pressure (bar)	1,16,18
Preheat Temperature Tu (K)	900,1100,1250
Equivalence ratio	0.3-1.0
Fraction of added fuel	0-100%

8 Numerical Results & Analysis

8.1 Introduction

The results of the simulations performed with the mechanism of Williams et al, the so-called San Diego mechanism are shown below.

8.2 Global Chemical Time

The laminar flame speed, and consequently the global chemical time scale depends on both preheat temperature, pressure and the diffusivity of the fuel. To visualize the effect of diffusion on the chemical time scale; a study of hydrogen added to a natural gas mixture and burned at constant flame temperature as shown in Figure 34 was included. With 80 % hydrogen by volume in natural gas the chemical time has decreased approximately by 75% compared to pure natural gas indicating a profound effect on the chemical reactions when adding a highly diffusive and light species such as hydrogen with a flame temperature of 1650K. For higher flame temperatures the effect of added hydrogen is smaller. At $T_f = 1850K$ the relative difference is roughly 50%.

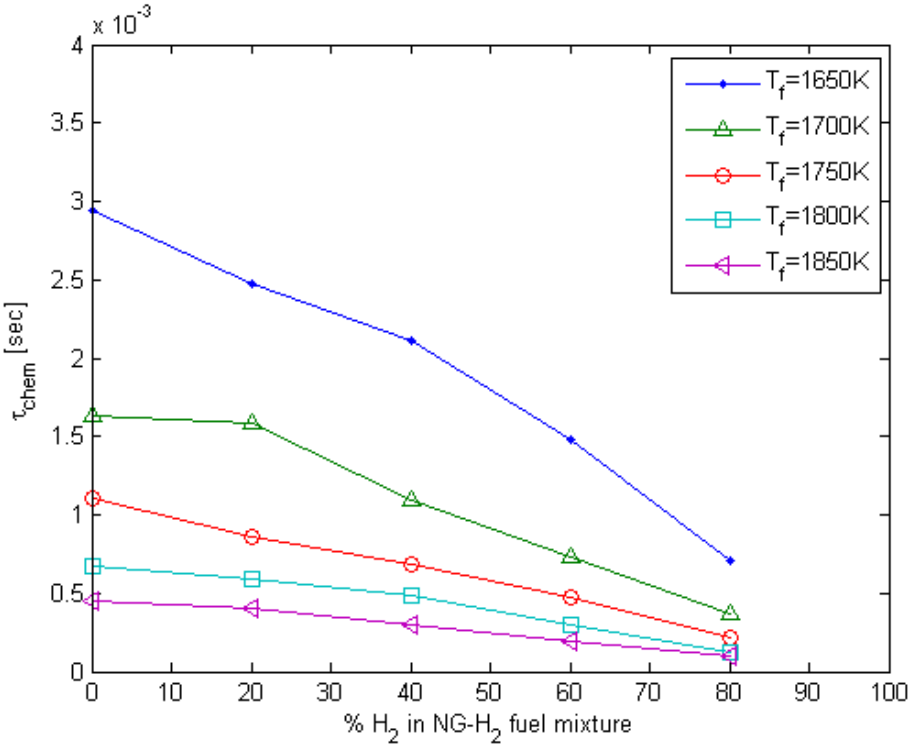

Figure 34. Global chemical time as a function of hydrogen content in a Natural Gas – Hydrogen fuel mixture burning in air for various adiabatic flame temperatures. $T_u = 693K$ *, P=16bar.*

Figure 35 and Figure 36 shows the effect on the global chemical time when adding different fuel components to natural gas at two constant flame temperatures 1650K and 1700K respectively. Apart from the effect of added hydrogen as shown in previous figures, adding carbon monoxide to natural gas will have a similar effect. Adding 80%

carbon monoxide by volume will decrease the chemical time by approximately 30 % at 1650K and 10-15% at 1700K. Despite keeping a constant flame temperature by which the effect of the diluent that absorbs heat is removed, adding an inert gas such as nitrogen will slow down the chemistry about 10 % indicating some secondary effect on the gas collision rates. At 1700K flame temperature (Figure 36) 80% carbon monoxide reduce the chemical time by approximately 20% whereas 80% nitrogen by volume would slow down the chemistry by 15-20%.

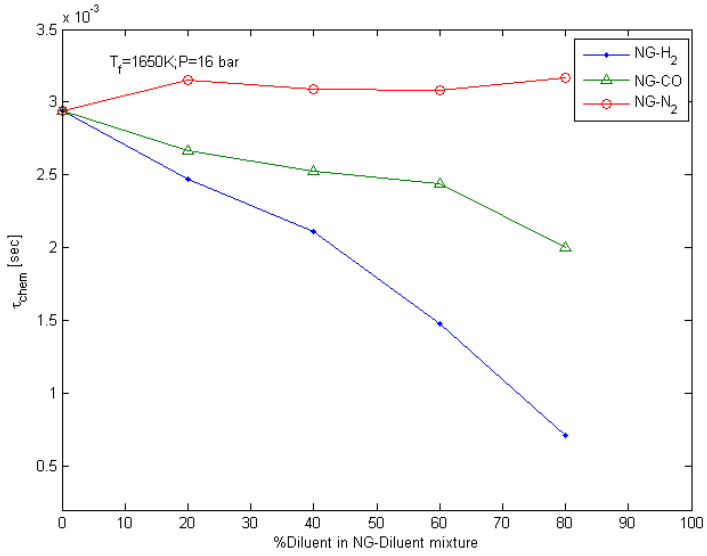

Figure 35. τ_{chem} *as a function of added fuel component in natural gas burning in air Tf=1650K, P=16 bar.*

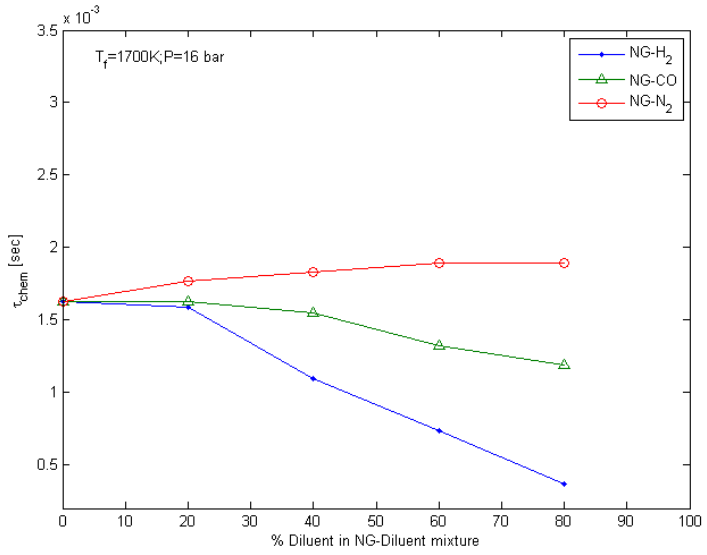

Figure 36. τ_{chem} *as a function of added fuel component in natural gas burning in air at Tf=1700K, P=16 bar.*

The figure below displays the global chemical time scale as a function of equivalence ratio and mixture composition $\alpha = \frac{x_{NG}}{x_{NG} + x_{N_2}}$ for a nitrogen-natural gas fuel mixture burning in air at P=1bar and a preheat temperature of 693K. The chemical time increases as the equivalence ratio is decreased as expected. For a fixed equivalence ratio the chemistry is clearly slowed down when adding more nitrogen. This is also the expected behavior when adding a diluent to the fuel. At gas turbine running conditions around $\phi = 0.5$ the dependence of added inert on the chemical time is relatively weak up to 50% inert by volume.

For very high nitrogen content ChemKin has a very bad convergence, hence only up to 80-90% dilution is shown here. It is reasonable to believe that a flammability limit would exist in the vicinity of this value for low equivalence ratios. The irregularities on the iso-contours are due to linear interpolation of non-converging points. The contours for all the graphs are based on 315 individual simulations, varying mixture fraction α and equivalence ratio ϕ independently in steps of 0.05.

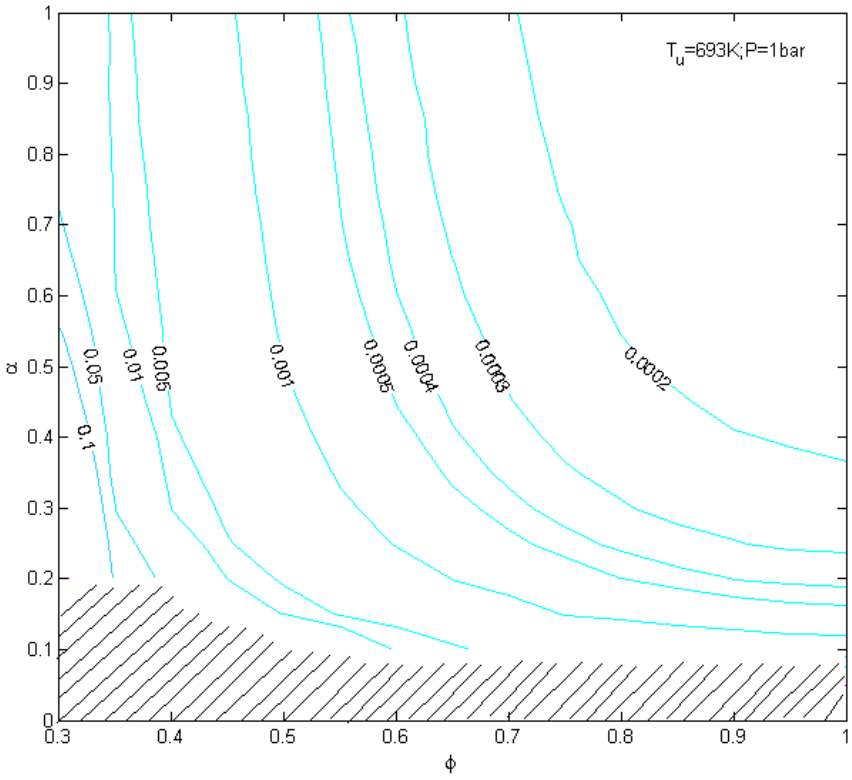

Figure 37. Global chemical time τ_{chem} [sec] as a function of equivalence ratio and mixture composition of a N2- natural gas fuel mixture burning in air. Preheat temperature Tu=693K, P=1 bar. Key: iso-contours – global chemical time.

Figure 38 displays the corresponding flame temperature to Figure 37 as a function of equivalence ratio and mixture composition. The flame temperature increases with increasing equivalence ratio as expected. The lowest flame temperature occurs for lean mixtures with high inert content and the highest for stoichiometric mixtures with low nitrogen content. For a fixed equivalence ratio, adding nitrogen will decrease the flame temperature about 100K up to approximately 60% nitrogen by volume, from 60% to 80% another 150K. Flame extinction eventually occurs for mixtures with more than 90% nitrogen for moderate to high equivalence ratios. For very lean mixtures extinction occurs earlier around 80-90% nitrogen by volume. The trend of the iso-contours of the chemical time and flame temperature might indicate a clear dependence between the two, thus the chemistry time scales are controlled by temperature rather than diffusion mechanisms.

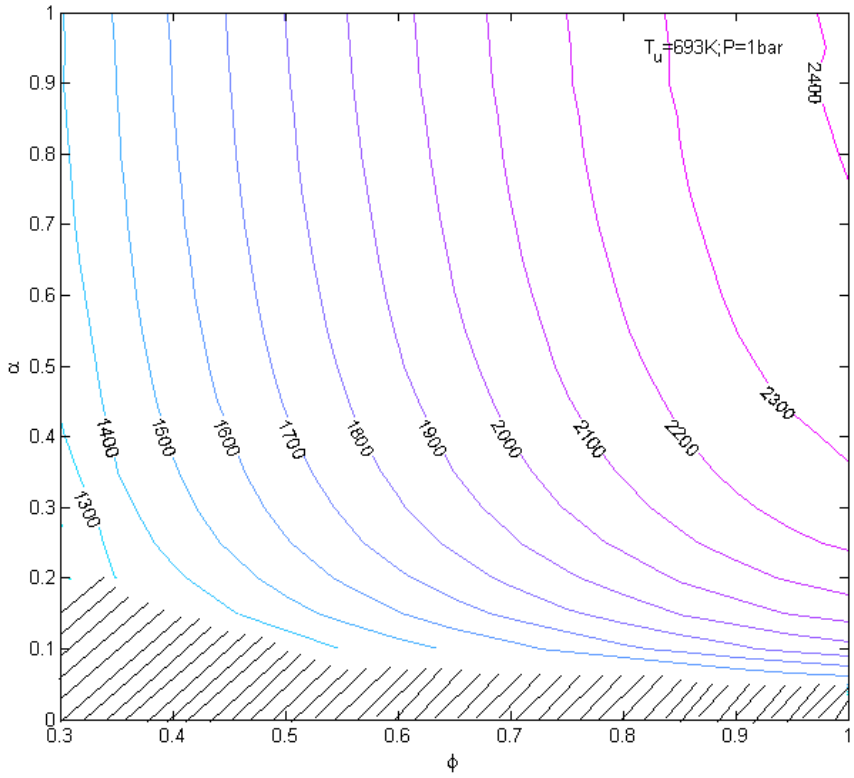

Figure 38. Iso-contours of flame temperature for varying equivalence ratio and mixture composition α for a N2-natural gas fuel mixture burning in air. P=1 bar; Tu=693K.

The behavior of the chemical time scale, when adding carbon dioxide to natural gas is shown in Figure 39, where $\alpha = \frac{x_{NG}}{x_{NG} + x_{CO2}}$. Similar to the nitrogen and natural gas mixture case in Figure 37 the chemical time increases with decreasing equivalence ratio. The trend of the iso-contours is similar to the nitrogen case. For a fixed mixture composition at an equivalence ratio close to 1, the chemical time becomes almost independent of the equivalence ratio. This effect is slightly more profound in the CO2 case compared to the nitrogen and natural gas case. At typical gas turbine running conditions around $\phi = 0.5$ the effect of added inert on the chemical time is fairly weak up to about 50% CO2, similar to the nitrogen case. From a chemical kinetics point of view no substantial change in the chemistry occurs below 50 % inert by volume. Since a typical gas turbine has a limited operational range in terms of equivalence ratio around $\phi = 0.5$, it would seem reasonable that a possible flameout may occur around 50% inert. The plot is produced out of 315 simulations similar to the previous mixture in Figure 37 and Figure 38.

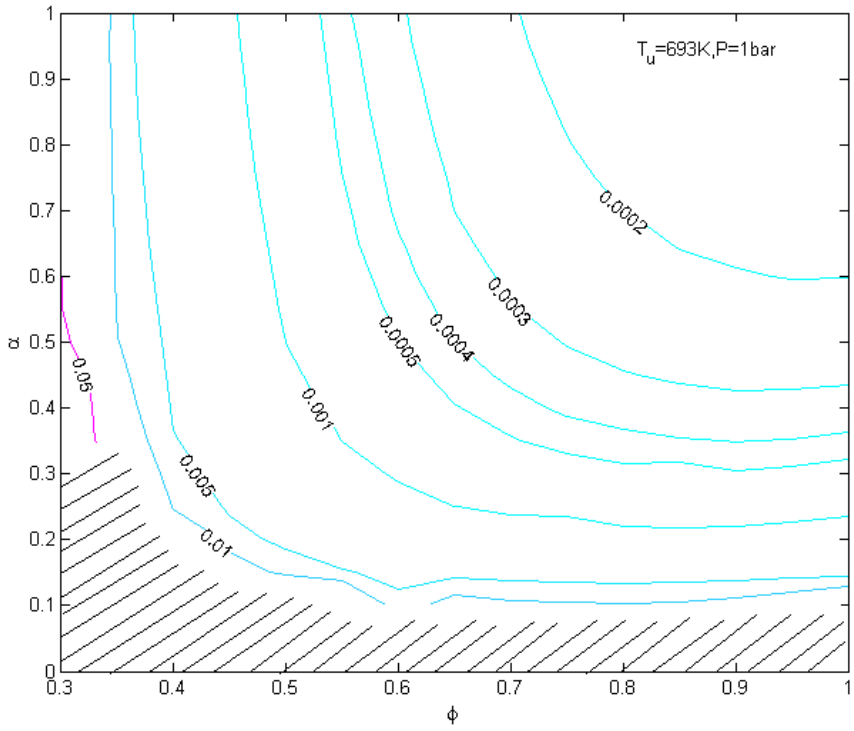

Figure 39. Global chemical time τ_{chem} [sec] as a function of equivalence ratio and mixture composition of a CO2- natural gas fuel mixture burning in air. Preheat temperature Tu=693K, P=1 bar. Key: iso-contours – global chemical time.

The corresponding flame temperature behavior is displayed in Figure 40. The trend is also very similar to the nitrogen – natural gas case in Figure 38. The similarities between the temperature trend and the chemical time trend indicate that the chemistry is controlled by temperature rather than by diffusion mechanisms. The slight differences between the nitrogen case and the carbon dioxide case are assumed to due to differences in heat capacities and the fact that CO2 is a major product of combustion and participate in several reaction steps.

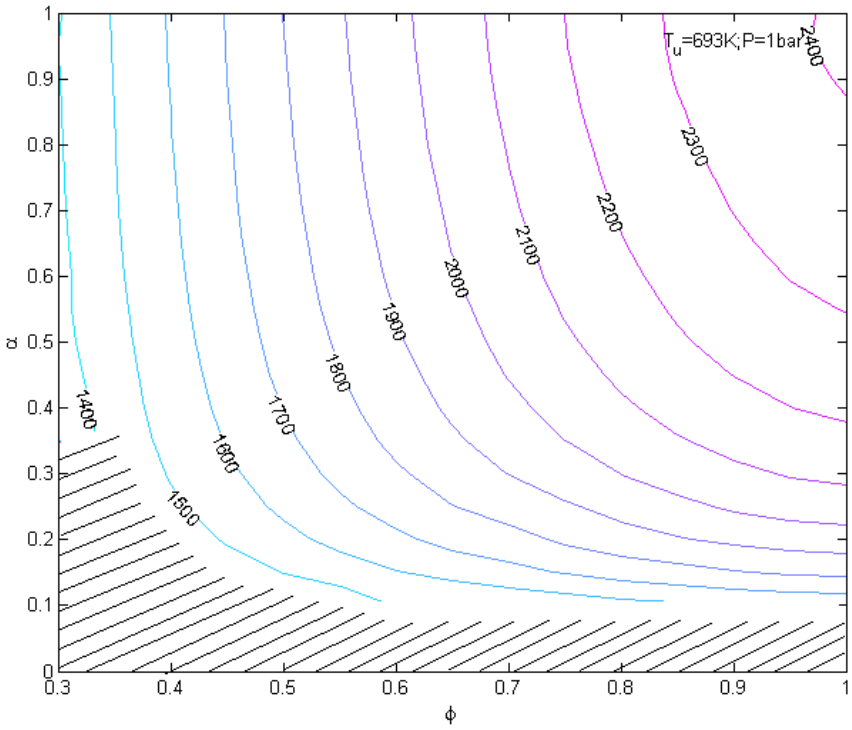

Figure 40. Iso-contours of flame temperature for varying equivalence ratio and mixture composition α for a CO2-natural gas fuel mixture burning in air. P=1 bar; Tu=693K.

Figure 41 show the global chemical time as a function of equivalence ratio and mixture composition $\alpha = \frac{x_{NG}}{x_{NG} + x_{H_2}}$ for a hydrogen-natural gas fuel mixture burning in air at P=16bar. Also here the chemical time increases as the equivalence ratio is decreased. The convergence of the ChemKin PREMIX code is however very poor in the vicinity of $\phi = 0.3$ which coincides with the approximate lean flammability limit located around $\phi = 0.27$. The fastest chemistry occurs for high H2 content around $\phi = 1$. The slope of the iso-contours indicates that for a fixed equivalence ratio the chemistry speeds up as the amount of hydrogen in the fuel mixture is increased on the contrary to adding inert gas. This might indicate a lowered flameout (or lean flammability) limit as more hydrogen is added. Experimentally, only flameback was observed when burning natural gas with hydrogen in the rig tests. From a strict chemical kinetics point of view the limit for flameback moves towards lower equivalence ratios as more hydrogen is added.

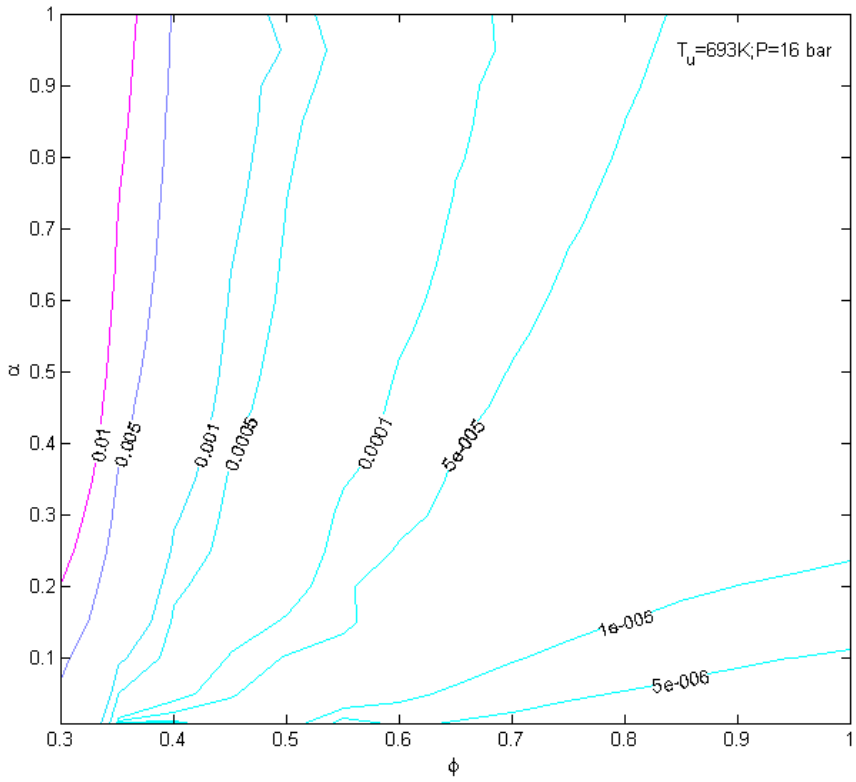

Figure 41. Global chemical time τ_{chem} [sec] as a function of equivalence ratio and mixture composition of a H2- natural gas fuel mixture burning in air. Preheat temperature Tu=693K, P=16bar. Key: iso-contours – global chemical time.

Figure 42 show the iso-contours of flame temperature for varying mixture composition and equivalence ratio. As expected the flame temperature increases with increased equivalence ratio. The increase due to increased amount of hydrogen in the fuel mixture is however weak, indicating that the effect of temperature on the laminar flame speed, hence the chemical kinetic time scale is small compared to diffusion effects. For an equivalence ratio of 0.5, increasing the hydrogen content from 0-100% will give a 100K increase in flame temperature. The behavior of the flame temperature does not follow the chemical time scale in Figure 41, indicating large effects of diffusion on the laminar flame speed.

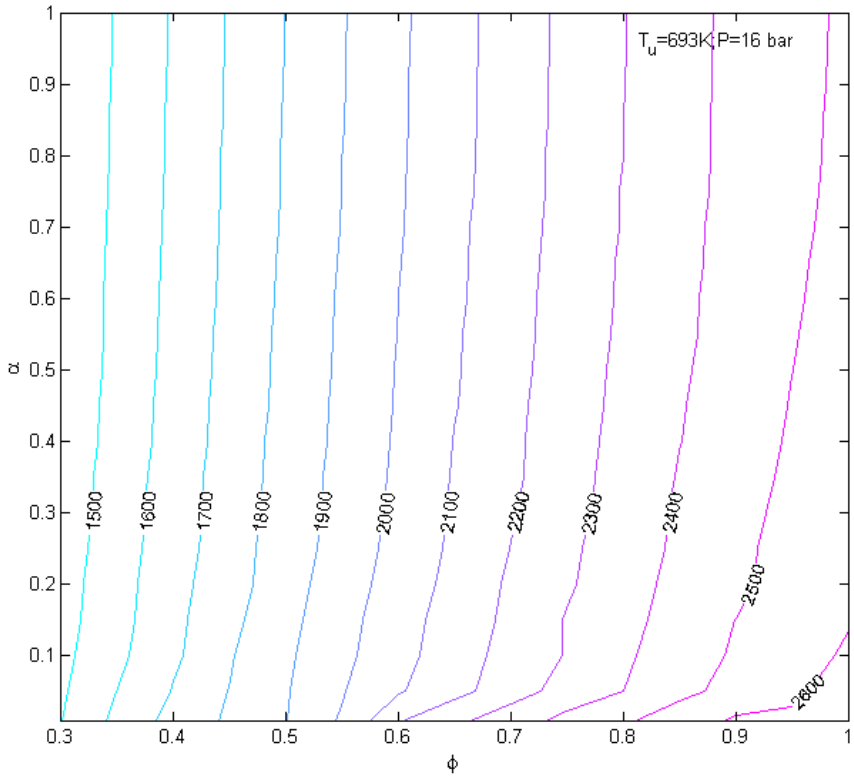

Figure 42. Iso-contours of flame temperature for varying equivalence ratio and mixture composition α for a H2-natural gas fuel mixture burning in air. P=16 bar; Tu=693K.

The chemical time scale of a carbon monoxide-natural gas fuel mixture burning in air as a function of equivalence ratio ϕ and mixture composition $\alpha = \frac{x_{NG}}{x_{NG} + x_{CO}}$ at 16 bar pressure with a preheat temperature of 693K is shown in Figure 43. The chemical time scale increases as the equivalence ratio is lowered. Similar to the H2 – natural gas case there is a weak trend that the chemistry speeds up for a fixed equivalence ratio when increasing the amount of carbon monoxide in the fuel mixture. At very high CO content the chemistry however slows down severely especially for equivalence ratios above 0.5. For 100% CO, PREMIX has a very poor convergence. Interestingly the carbon monoxide on itself seems to react very slowly whereas in interaction with methane, ethane and propane, the behavior is the opposite. Carbon monoxide is an unstable intermediate species. On itself it dissociate slowly whereas in interaction with natural gas the chemistry speeds up due to the existence of H and OH radicals in the mixture, which speeds up the oxidation of CO through elementary reactions such as $CO + OH = CO_2 + H$. Similarly, the plot is based on 315 individual simulations.

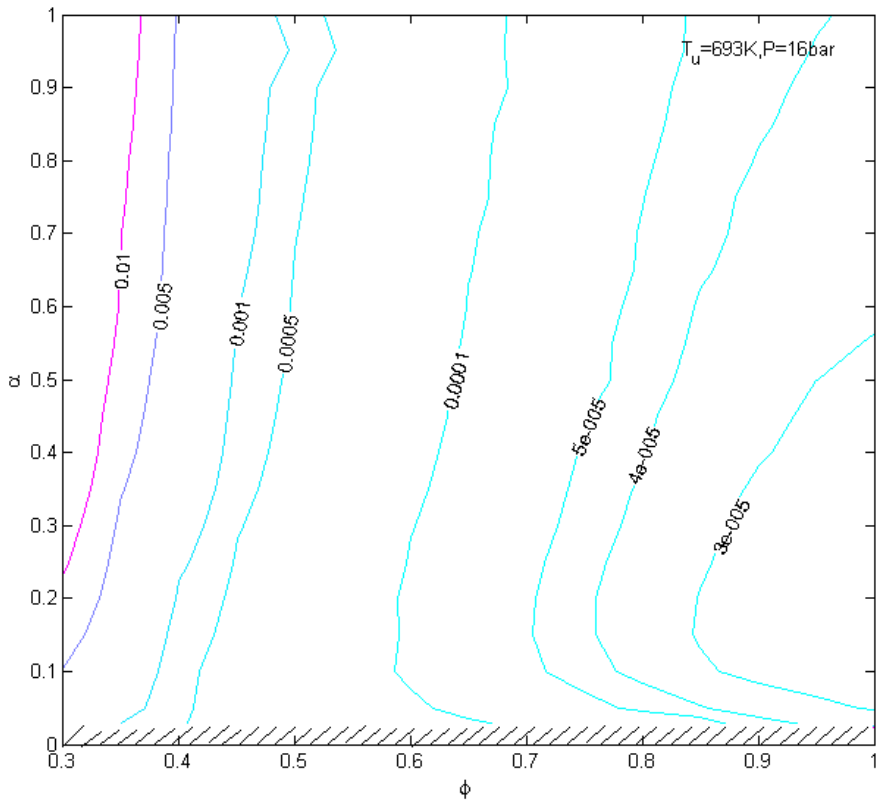

Figure 43. Global chemical time τ_{chem} [sec] as a function of equivalence ratio and mixture composition of a CO natural gas fuel mixture burning in air. Preheat temperature Tu=693K, P=16bar. Key: iso-contours – global chemical time.

Figure 44 shows the flame temperature of Figure 43 for the conditions stated with a clear trend of decreasing flame temperature as the equivalence ratio is lowered. For a fixed equivalence ratio increasing the CO fraction in the fuel mixture will lead to an increase in flame temperature. The maximum flame temperature occurs in high CO content mixtures at stoichiometric conditions. For a fixed equivalence ratio around $\phi = 0.5$, increasing the CO amount from 0% to 100% will result in a 200K increase in flame temperature.

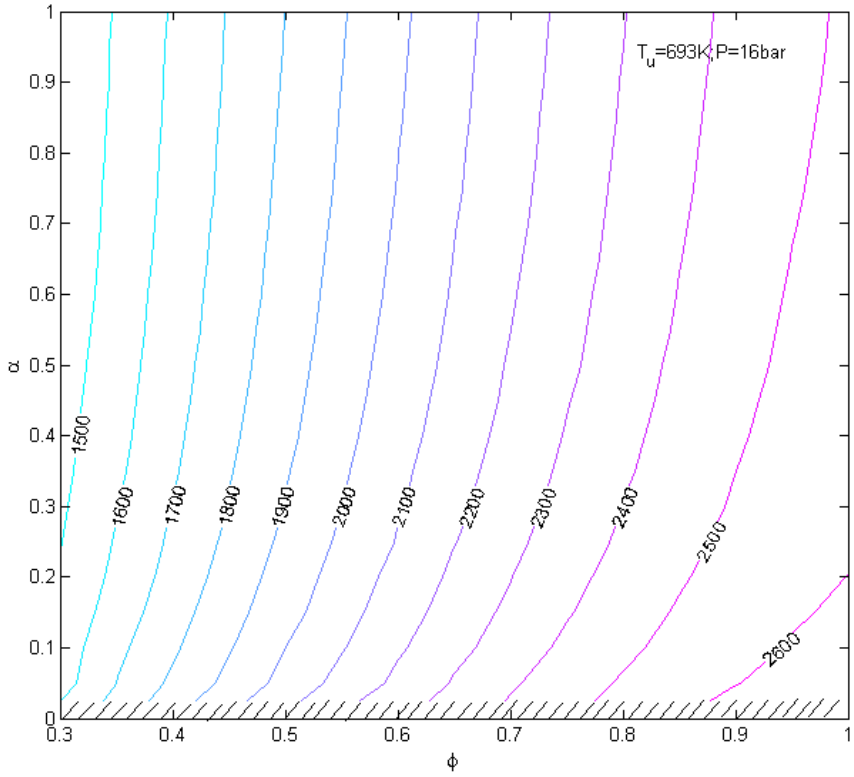

Figure 44. Iso-contours of flame temperature for varying equivalence ratio and mixture composition α for a CO-natural gas fuel mixture burning in air. P=16 bar; Tu=693K.

Figure 45 displays the chemical time for varying 50:50 H2:CO syngas-natural gas mixture composition $\alpha = \frac{x_{NG}}{x_{NG} + x_{syngas}}$ and equivalence ratio at a higher pressure P=18 bar. No profound effect on the chemical time scale can be seen when comparing pure natural gas at 16 and 18 bar pressure ($\alpha = 1$). The increase of the laminar time scale is evident as the equivalence ratio is decreased, approaching the lean flammability limit. The iso-contours of the global chemical time are displaced further to the lean side when the amount of syngas in the syngas-natural gas mixture is increased. With a fixed operational range of equivalence ratio this means that the margin to flashback at a given burner configuration and flow conditions should decrease with increasing syngas content in the fuel mixture. A possible flameout limit would then be displaced towards lower equivalence ratio. The behavior of the chemical time scale is similar to the H2-natural gas case in Figure 41 for equivalence ratios around 0.5. Only for very lean ($\phi < 0.3$) and richer ($\phi > 0.7$) mixtures the inhibiting effect of CO can be seen. 315 individual simulations were required.

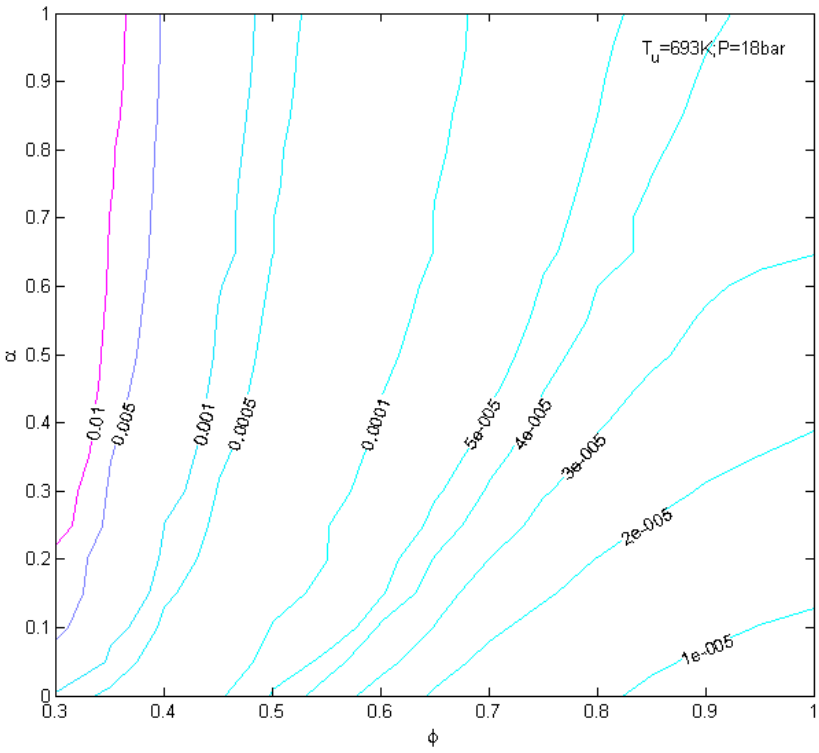

Figure 45. Global chemical time τ_{chem} [sec] as a function of equivalence ratio and mixture composition. 50:50 H2:CO syngas co-firing with natural gas in air. Preheat temperature Tu=693K, P=18bar. Key: iso-contours – global chemical time.

The effect of fuel mixture and equivalence ratio on the flame temperature can be seen in Figure 46. For lean mixtures the flame temperature is low and increases with increased equivalence ratio as expected. For a given equivalence ratio the flame temperature increases somewhat with increasing syngas content in the fuel mixture. From 0-100% syngas the flame temperature increases by approximately 200K at $\phi = 0.5$. Compared to the H2-natural gas case in Figure 42 carbon monoxide increases the flame temperature somewhat. Note however the increase in pressure to 18bar.

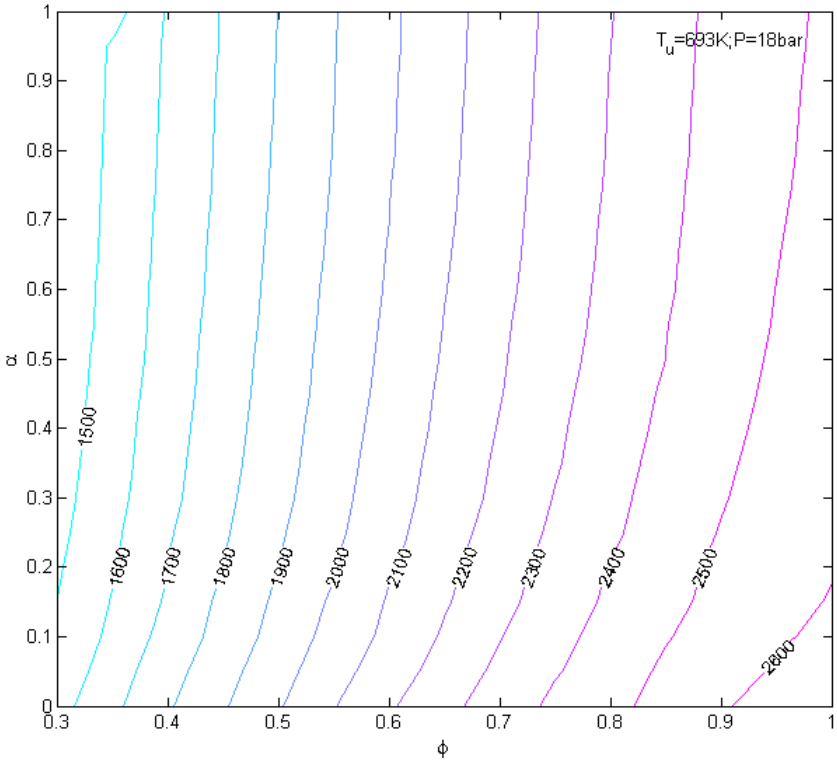

Figure 46. Flame temperatures for varying equivalence ratio and mixture composition. 50:50 H2:CO syngas co-firing with natural gas in air. Preheat temperature Tu=693K, P=18bar. Key: iso-ccontours – flame temperature.

8.3 Ignition delay

The effect of added nitrogen to natural gas on the ignition delay is shown in Figure 47. Similar to the previous graphs in section 8.2 the mixture composition is denoted by $\alpha = \frac{x_{NG}}{x_{NG} + x_{N_2}}$ and equivalence ratio by ϕ. Similarly to the global chemical time investigation, one contour plot consists of 315 simulated data points. The preheat temperature is determined according to Appendix 0. For atmospheric conditions and a preheat temperature of 1250K the ignition delay time is not a strong function of the amount of nitrogen except for very high N2 concentrations. The slight incline of the contours however indicate that leaner mixtures actually have a shorter ignition delay time than for high equivalence ratios. Since nitrogen is an inert gas this behavior is believed to be caused by inaccurate temperature dependence of the reaction rates. Above 90% N2 by volume the ignition delay time increases severely and eventually approaches infinity (hashed area). For high nitrogen concentrations the ignition delay time is practically independent of the equivalence ratio.

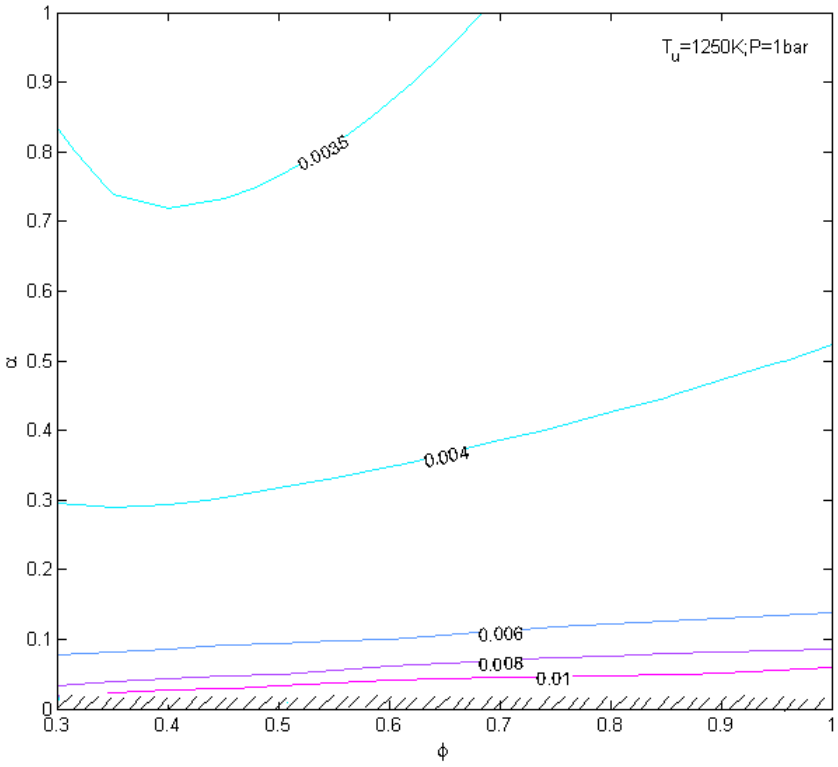

Figure 47. Ignition delay time τ_{ig} [sec] as a function of mixture composition α and equivalence ratio for a N2-natural gas fuel mixture burning in air at P=1bar, Tu=1250K. Key: iso-contours – ignition time

The dependence of the ignition delay time on mixture composition and equivalence ratio of a natural gas and carbon dioxide fuel mixture burning in air at atmospheric pressure, $T_u = 1250K$ is shown in Figure 48, $\alpha = \frac{x_{NG}}{x_{NG} + x_{CO_2}}$. The behavior of the ignition delay time is very similar to the N2-NG mixture case. However a stronger dependence of the equivalence ratio can be seen for moderate to high CO2 content. In the case of carbon monoxide the behavior can be explained by the fact that CO2 is a major product of combustion and is part of several reaction steps.

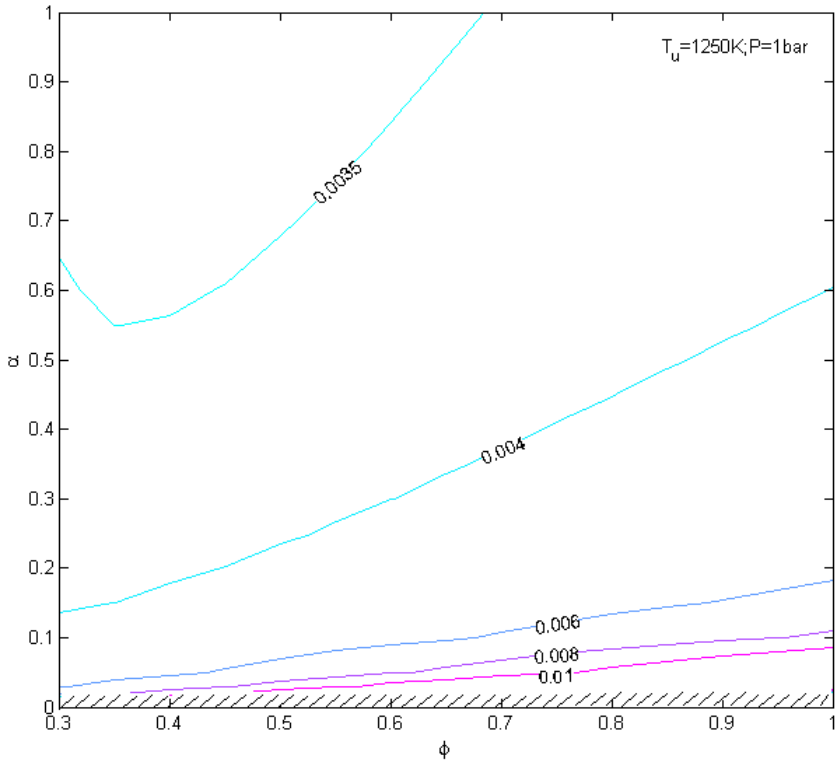

Figure 48. Ignition delay time τ_{ig} [sec] as a function of mixture composition α and equivalence ratio for a CO2-natural gas fuel mixture burning in air at P=1bar, Tu=1250K. Key: iso-contours – ignition time

The ignition delay time of a hydrogen – natural gas fuel mixture burning in air at high pressure P=16 bar, $T_u = 1100K$ as a function of equivalence ratio and mixture composition $\alpha = \frac{x_{NG}}{x_{NG} + x_{H_2}}$ is shown in Figure 49. The ignition delay time decreases with increasing hydrogen content in the fuel. The dependence of the equivalence ratio is also quite profound. From a chemical kinetic point of view, at the running conditions stated the range of operation, taking flashback into account, is highly limited. At $\phi = 0.5$ the ignition delay time is around 3.5 msec for pure natural gas and by only adding 35% hydrogen the ignition delay time is decreased to around 2 msec. At 80% hydrogen in natural gas the ignition time is around 1 msec. It is however unclear what exactly causes a flashback/flameback which is also likely to depend on the fluid dynamic properties of the fuel/air mixture.

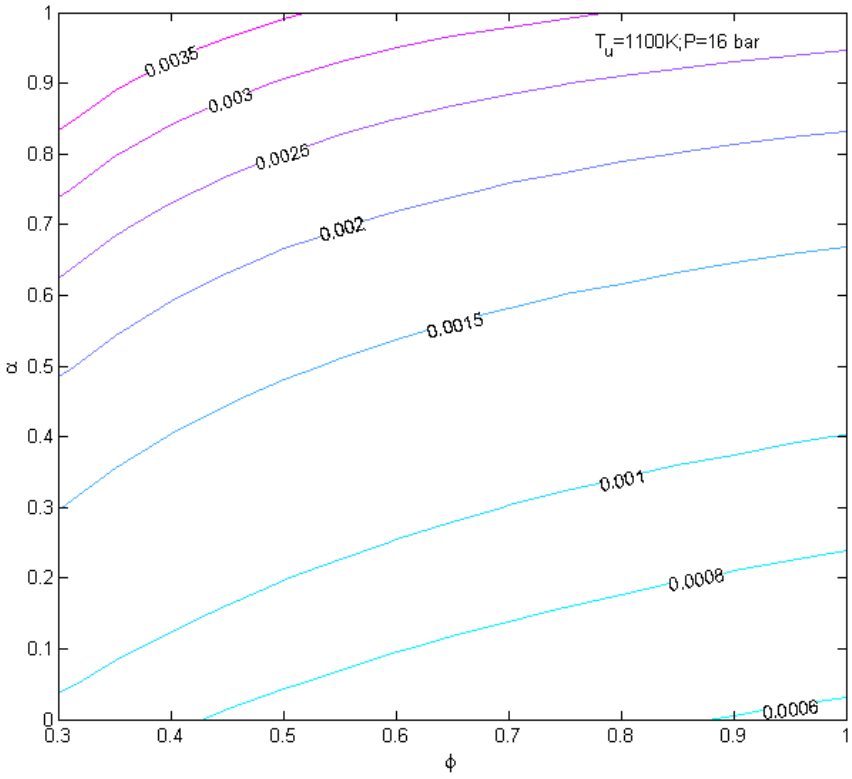

Figure 49. Ignition delay time τ_{ig} [sec] as a function of mixture composition α and equivalence ratio for a H2-natural gas fuel mixture burning in air at P=16bar, Tu=1100K. Key: iso-contours – ignition time

Adding carbon monoxide to natural gas will also increase the risk of flameback/flashback as shown in Figure 50 where $\alpha = \frac{x_{NG}}{x_{NG} + x_{CO}}$. At low to moderate CO levels the dependence of the mixture composition on the ignition time is not as strong as in the hydrogen case, i.e. for a fixed equivalence ratio a higher CO content is allowed before the ignition delay changes remarkably. For ignition times between 2.5 and 3 msec the slope of the contour curve suddenly changes. For moderate to high CO levels from about 60-98%, the behaviour of the ignition delay time is similar to the hydrogen case. The magnitude of the ignition delay time is generally larger but the dependence of the equivalence ratio is similar. For very high CO content (above 98%) the iso-contours indicate a sudden abrupt increase of the ignition delay time, closing in on 100% CO. Pure CO has an ignition delay time roughly 1000 times longer than at 98% CO 2%NG.

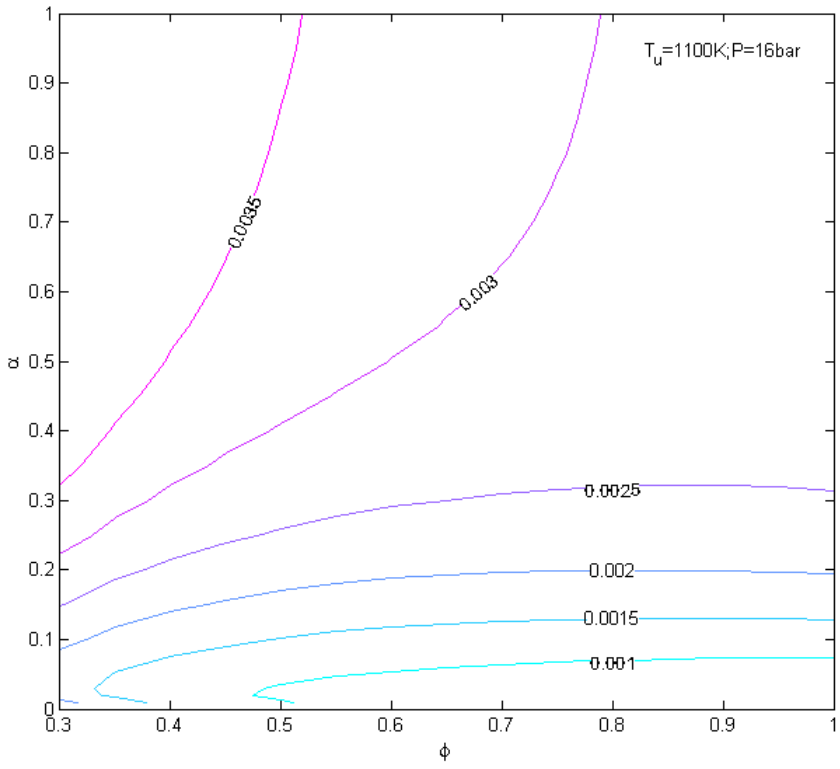

Figure 50. Ignition delay time τ_{ig} [sec] as a function of mixture composition α and equivalence ratio for a CO-natural gas fuel mixture burning in air at P=16bar, Tu=1100K. Key: iso-contours – ignition time

Figure 51 shows the ignition delay time as a function of mixture composition $\alpha = \frac{x_{NG}}{x_{NG} + x_{syngas}}$ and equivalence ratio for a 50:50 H2:CO syngas co-firing with natural gas in air at P=18 bar and preheat temperature $T_u = 1100K$ .The similarity with H2 and natural gas mixture in Figure 49 is clear, hence hydrogen seems to dominate over carbon monoxide. The ignition delay time is of the same order as the hydrogen and natural gas mixture case, with some differences for high syngas content and high equivalence ratio.

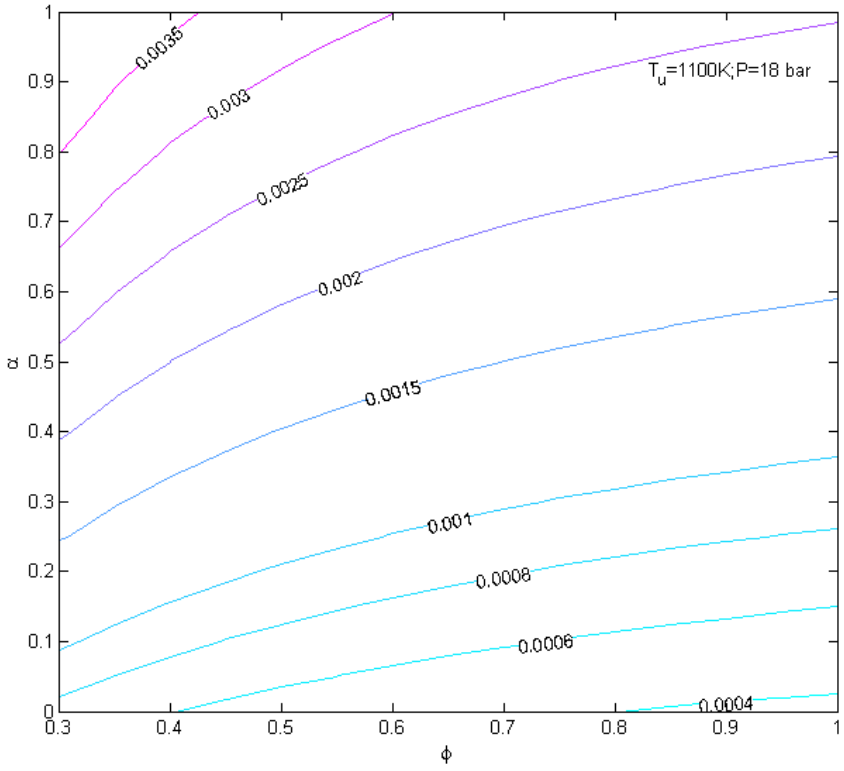

Figure 51. Ignition delay time τ_{ig} [sec] as a function of mixture composition α and equivalence ratio for a 50:50 H2:CO-natural gas fuel mixture burning in air at P=18bar, Tu=1100K. Key: iso-contours – ignition time

Lowering the preheat temperature obviously results in longer ignition delay time. At a preheat temperature of 900K an interesting interaction between hydrogen and natural gas occurs as shown in Figure 52. The ignition delay time, several orders of magnitude larger than at 1100K increases as the equivalence ratio is lowered as expected. There is however a trend of increasing delay time with added hydrogen content up to about 50% H2 by volume. As the H2 content is further increased the ignition delay again decreases. The shortest ignition delay time is around 80-90 msec for pure hydrogen around stoichiometry. Decreasing the equivalence ratio increases the ignition delay time up to around 140 msec at $\phi = 0.3$. These time scales are several orders of magnitude larger than the approximate critical time scale for flameback for the LB000 burner at the rig test conditions.

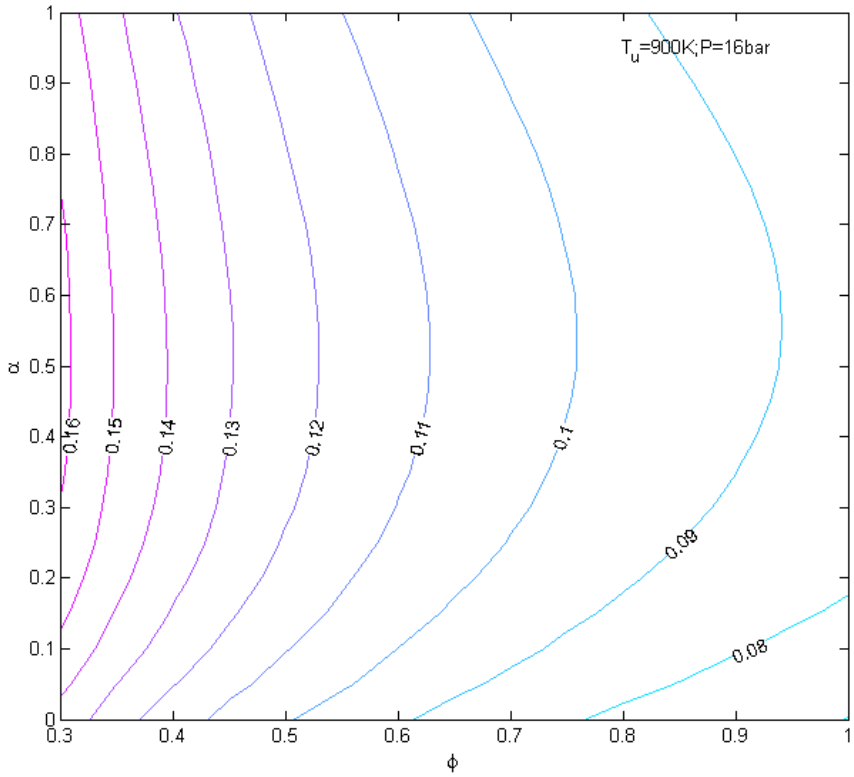

Figure 52. Ignition delay time τ_{ig} [sec] as a function of mixture composition α and equivalence ratio for a H2-natural gas fuel mixture burning in air at P=16bar, Tu=900K. Key: iso-contours – ignition time

8.4 Conclusions & Discussion

Using the chemical kinetic mechanism of Williams et al, the so-called San Diego mechanism the numerical predictions show the global chemical time scale as one way of characterizing the chemical kinetic behavior of a gas mixture.

As expected adding inert species such as nitrogen and carbon dioxide affects the chemistry mostly as a corresponding decrease in temperature. For a fixed flame temperature there is however a very small trend of an increased chemical time. Whether this is due to a systematic numerical error is unknown. Observations of a slight change in the position of the laminar flame front and the gradients have been made when going to very low equivalence ratios. This could result in a non-zero temperature or species gradient at the cold boundary and consequently errors in the predictions. However, increasing the inert content would rather require an increased equivalence ratio to maintain flame temperature.

Attempts to correlate the chemical time with a limit for flameout for the different gas mixtures were made. Below Figure 37 is reproduced with corresponding rig test data points up to 35% nitrogen by volume. The triads indicate test runs where flameout occurred for the given burner. Circles represent finished runs with a maintained stable flame. In this mixture interval it is reasonable to believe that the chemical time scale approximate the limit for flameout quite well at atmospheric pressure. In this interval the limit for the given LB000 reference burner is approximately 1 msec. At even higher nitrogen content it is believed that other burner specific fluid dynamic effects become

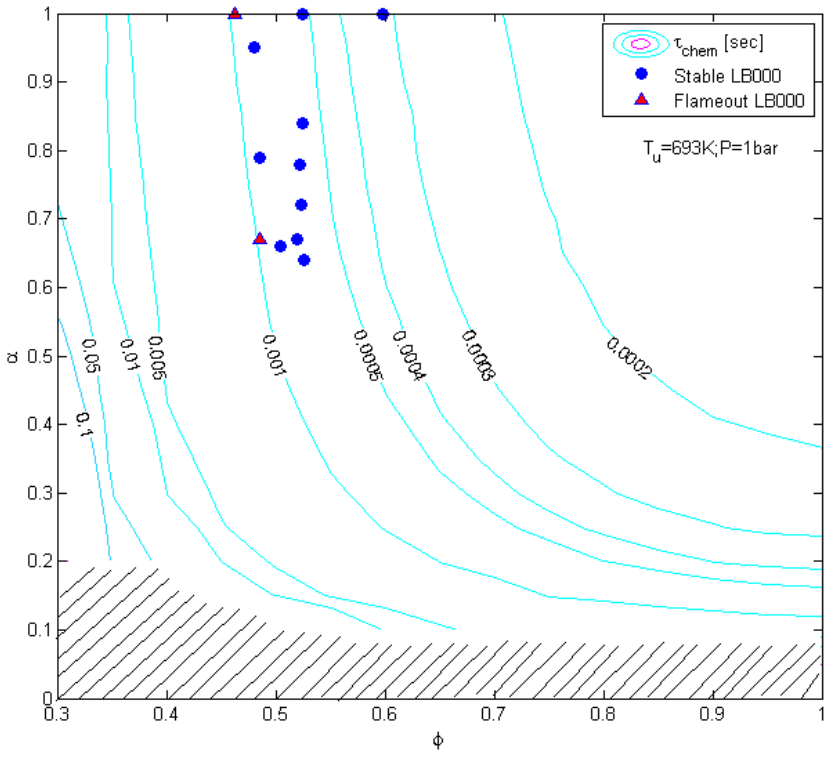

Figure 53. Figure 37 showing $\tau_{chem}[\mathrm{sec}]$ co-plotted with flameout rig test data.

important and therefore not shown here due to company secrecy. The burner pressure drop may change resulting in a change in the cooling conditions. High inert content may affect the turbulence intensity as well as the mixing of air and fuel in the mixing tube, hence creating mixture inhomogeneties that affect the flame.

Similar comparisons were made for the other fuel mixtures. A somewhat similar trend could be found for the CO2-natural gas mixture.

The behavior of the auto ignition delay time as a function of equivalence ratio and mixture composition is of general interest, although not an issue at the current rig operating conditions. The ignition delay is weakly affected by increased inert content. Above 85% inert content by volume (N2 or CO2) the ignition delay time scale starts to increase more abruptly. With operating conditions where auto ignition is an issue adding inert gas would obviously increase the margin against flashback. For both N2 and CO2, above 85% inert content the ignition delay is nearly independent of the equivalence ratio.

In adding hydrogen or carbon monoxide the chemistry is greatly affected. Both species, with completely different behavior when burned alone, interact with natural gas and speeds up the chemistry. For lean mixtures and low to moderate values of α, the behavior of the chemical time is very similar for both H2-NG, CO-NG and the 50:50 H2:CO syngas-NG fuel mixture. Major differences appear for $\alpha > 0.9$ with the carbon monoxide increasing the chemical time severely. At high pressure it is reasonable to believe that certain fluid dynamic mechanisms become more important for moderate to high values of α similar to the atmospheric cases. Clear conclusions cannot be made due to insufficient amount of available high pressure rig test data. Comparing flame temperatures; the CO-NG and syngas-NG mixtures will produce an increase in flame temperature twice as large as the H2-NG mixture from 0% to 100% CO/syngas/H2 respectively. This further confirms the diffusive nature of hydrogen, speeding up the chemistry through diffusion rather than high temperature.
In the case of auto ignition it is clear that hydrogen will support a flameback, given a sufficiently high preheat temperature. In this case the range of operation would be highly restricted. At a lower temperature the behavior can however be quite different. In adding carbon monoxide the risk of a flameback may also increase if the equivalence ratio is sufficiently high. For the syngas case at the conditions stated the range of operation is further decreased.
To elucidate the difference between the chemical time scale and the ignition delay time scale, a summary is presented in Figure 54 for an equivalence ratio of 0.5 and mixture fraction $\alpha = 0.5$. For all preheat temperatures the difference is several orders of magnitude. The pressure dependence has to be considered weak.

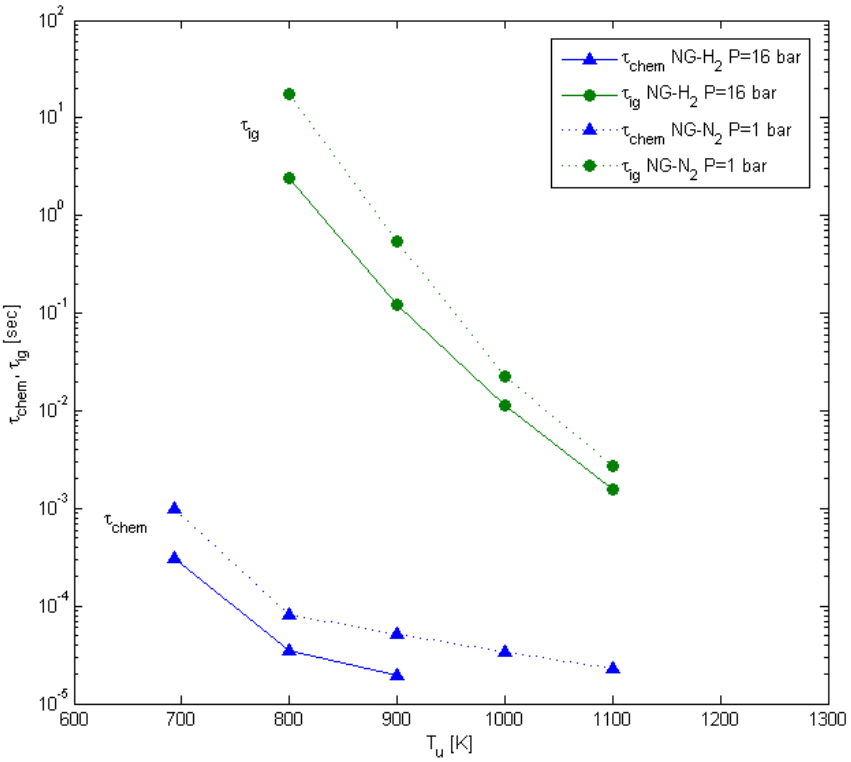

Figure 54. Comparisons of the magnitude of the global chemical time scale τ_{chem} and the ignition delay time scale τ_{ig} for varying air preheat temperature

It is reasonable to believe that, given a sufficiently high preheat temperature; flameback supported by auto ignition is a highly relevant mechanism. At typical SIT gas turbine running conditions (LB000 burner running conditions, 3 msec residence time) the ignition delay time approaches infinity, hence the flameback phenomena is not supported by auto ignition but rather due to fluid dynamic effects such as vortex breakdown in the recirculation zone.

9 Concluding Remarks

The development of the numerical model and the subsequent numerical investigations has resulted in the following conclusions:

All the chemical kinetic mechanisms predict laminar flame speed quite well for lean mixtures at ambient conditions.

With increasing preheat temperature the discrepancies increase against measurements indicating inaccurate temperature dependence of rate coefficients for all the mechanisms tested.

None of the mechanisms tested are really suitable for predicting laminar flame speeds of pure syngas mixtures. For applications with natural gas co-firing; the mechanism of Williams et al is considered to produce adequate results.

Experimental laminar flame speed data at high pressure with air as an oxidizer is highly limited. The use of oxygen-helium data was necessary for validation at gas turbine operating conditions.

For ignition delay time calculations both the Plug-Flow Reactor and the Homogeneous Constant Pressure Reactor produce similar results. The key difference in predictions is the definition of the ignition delay time. Using the maximum temperature gradient is the preferred way to calculate the ignition delay time.

Cantera consistently over-predict laminar flame speed compared to ChemKin for the mixtures included in this study. Slight differences in the grid refinement parameters might explain the difference. The discrepancies decrease with increased pressure. For ignition delay simulations with a closed homogeneous reactor model, Cantera produce the same result as ChemKin.
The Cantera code is more flexible than ChemKin but is associated with convergence instabilities and more numerical troubleshooting due to the lack of code documentation.

ChemKin is the preferred software when user friendliness and quick problem setup is taken into account. The ChemKin code is also more numerically robust than the Cantera code.

The global chemical time scale is a relevant fuel mixture characteristic and has been successfully correlated with the flameout limit for nitrogen - natural gas up to 35% nitrogen by volume at atmospheric pressure. A similar correlation was found for carbon monoxide – natural gas mixtures.

For very high inert content; other fluid dynamic effects become important and the stability limit is rather controlled by the specific burner design and flow- and cooling conditions.

Carbon monoxide, being an intermediate species shows an interesting behavior in supporting the chemical reactions when added to natural gas and decreasing the chemical time scale. Alone the dissociation is very slow due to the absence of a H and OH radical pool. This is particularly evident for the auto ignition mechanisms.

It is reasonable to believe that, given a sufficiently high preheat temperature flameback, supported by auto ignition is a highly relevant mechanism when adding hydrogen or carbon monoxide to natural gas. At the LB000 operating conditions auto ignition is however irrelevant, confirming that the observed flameback is caused by fluid dynamic effects.

10 Applications and suggestions for continued work

The numerical model developed will be useful in future simulations of fuel mixture characteristics. This report is therefore supposed to act as a reference when setting up new problems. The subsequent investigation of the global chemical time scale and the way it is presented will hopefully visualize the kinetic behavior of a fuel gas mixture and the approximate operational range of an arbitrary burner to a certain degree. This can possibly be used as guidance in future experimental work on fuel flexibility.

To be able to make proper correlations for flameout and flashback of hydrogen/carbon monoxide/syngas fuel mixtures, further experimental work in the rig would be useful. By using a more systematic approach the possible flameout limit could be better resolved in fewer test runs.
It would also be of great interest to obtain velocity fields of specific burners from either CFD or water rig tests to be able to estimate the turbulent time scales and possibly limits for flameout and flameback.

11 Literature references

[1] Warnatz, J., Maas, U. and Dibble, R. W., 2006, "Combustion: physical and chemical fundamentals, modeling and simulation, experiments, pollutant formation", 4th edition, Berlin, Springer.

[2] Schmidt, Lanny D., 1998, "The Engineering of Chemical Reactions", New York: Oxford University Press.

[3] Kee, R. J., et al., CHEMKIN Release 4.1, 2006, Reaction Design, San Diego CA.

[4] Borman, G. L., Ragland, K. W., 1998, "Selected Material from Combustion Engineering ME 140 Combustion Processes University of California-Berkeley", San Francisco, McGraw -Hill

[5] X-S. Bai, Professor, Department of Energy Sciences, Lund University, Private communication October 6th 2008.

[6] Noble, D. R., Zhang, Q., Shareef, A., Tootle, J., Meyers, A., Lieuwen, T., "Syngas Mixture Composition Effects upon Flashback and Blowout", ASME Paper No. GT2006-90470.

[7] Lieuwen T., McDonell, V., Petersen, E., and Santavicca, D., "Fuel Flexibility Influences on Premixed Combustor Blowout, Flashback, Autoignition and Stability," Journal of Engineering for Gas Turbines and Power, January 2008.

[8] X-S. Bai, Professor, Department of Energy Sciences, Lund University, Private communication September 4th 2008.

[9] Davis, S. G., Joshi, A. V., Wang, H., and Egolfopoulos, F., "An Optimized Kinetic Model of H2/CO Combustion", Proc. Combustion Institute, 2005. **30**: p1283-1292

[10] Sun, H., Yang, S. I., Jomass, G., and Law. C. K., "High Pressure Laminar Flame Speeds and Kinetic Modelling of Carbon Monoxide/Hydrogen Combustion." Proceedings of the Combustion Institute, 2007. **31**: p.439-446.

[11] Li, J., Zhao, Z., Kazakov, A. and Dryer, F., "An updated comprehensive kinetic model of hydrogen combustion.", International Journal of Chemical Kinetics, 2004. **36**(10): p.566-575

[12] Skreiberg, Ö., Kilpinen, P., and Glarborg, P., "Ammonia chemistry below 1400 K under fuel-rich conditions in a flow reactor, Combustion and Flame, ", 2004. **136:** p. 501-518.

[13] Smith, G. P., Golden, D. M., Frenklach, M., Moriarty, N. W., Eiteneer, B., Goldenberg, M., Bowman, C. T., Hanson, R. K., Song, S., Gardiner, W. C., Lissianski, V. V. and Qin, Z., GRI-mech3.0 <http://www.me.berkeley.edu/gri-mech/>

[14] Williams, F.A. et al., <http://maeweb.ucsd.edu/combustion/cermech/>

[15] Konnov, A.A., Detailed reaction mechanism for small hydrocarbons combustion. Release 0.4 <http://homepages.vub.ac.be/~akonnov/ >,1998.

[16] Saxena, P. and Williams, F. A., "Testing a small detailed chemical-kinetic mechanism for the combustion of hydrogen and carbon monoxide", Combustion and Flame, 2006. **145:** p. 316-323.

[17] Natarajan, J., Kocharm Y., Lieuwen, T., and Seitzman, J., 2008, "Laminar Flame Speed Measurements of H2/CO/CO2 Mixtures Up to 15 atm 600 K Preheat Temperature", ASME Paper No. GT2008-51364, 2008.

[18] Mclean, I. C., Smith, D. B., and Taylor, S. C., "The Use of Carbon Monoxide/Hydrogen Burning Velocities to Examine the Rate of the CO+OH Reaction", Proc. Combust. Inst, 1994. p.749-757.

[19] Andrews, G.E. and Bradley, D., "The Burning Velocity of Methane-Air Mixtures", Combustion and Flame, 1972. **19:** p. 275.

[20] Petersen, E. L., Hall, J. M., Smith, S. D., de Vries, J., Amadio, A. and Crofton, M. W., 2005, "Ignition of lean Methane-Based Fuel Blends at Gas Turbine Pressures", Proc. ASME Turbo Expo 2005, GT2005-68517, 2005.

[21] Tillmark, C., Dept. of Energy Sciences, Lund University, Sweden. Report: LUTMDN/TMHP-06/5093-SE, 2006.

Appendices

A Selecting a chemical kinetic mechanism

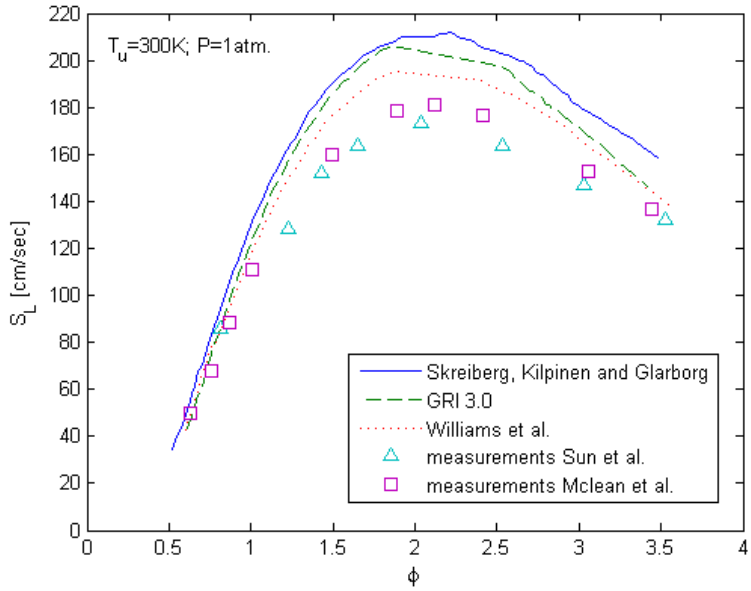

Figure 1. Laminar flame speeds for varying equivalence ratio of a 50:50 CO:H2 fuel mixture in atmospheric air at 300K. Key: Lines – simulations; symbols – measurements.

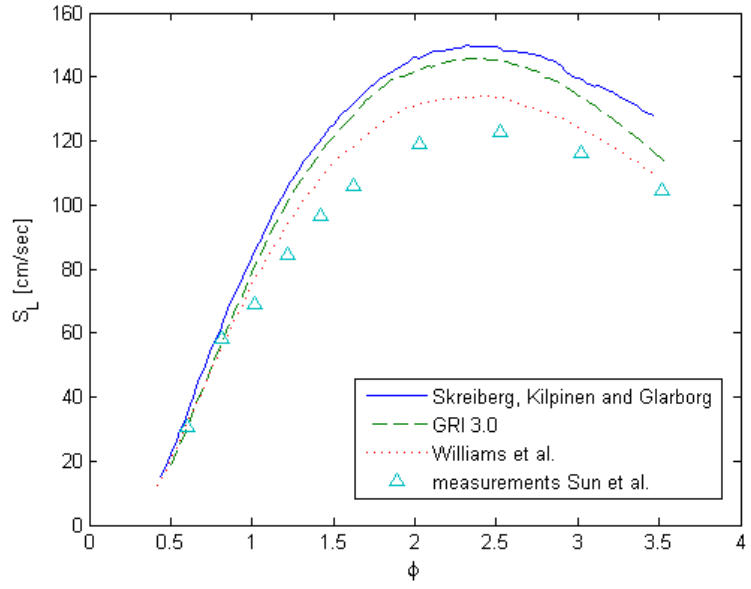

Figure 2. Laminar flame speeds for varying equivalence ratio of a 75:25 CO:H2 fuel mixture in atmospheric air at 300K, P=1atm. Key: Lines – simulations; symbols – experiments

B Standard Natural Gas Approximation

Laminar flame speed prediction for varying equivalence ratio approximating natural gas as pure methane and a methane-ethane-propane mixture respectively. The relative error is approximately 15% around stoichiometry.

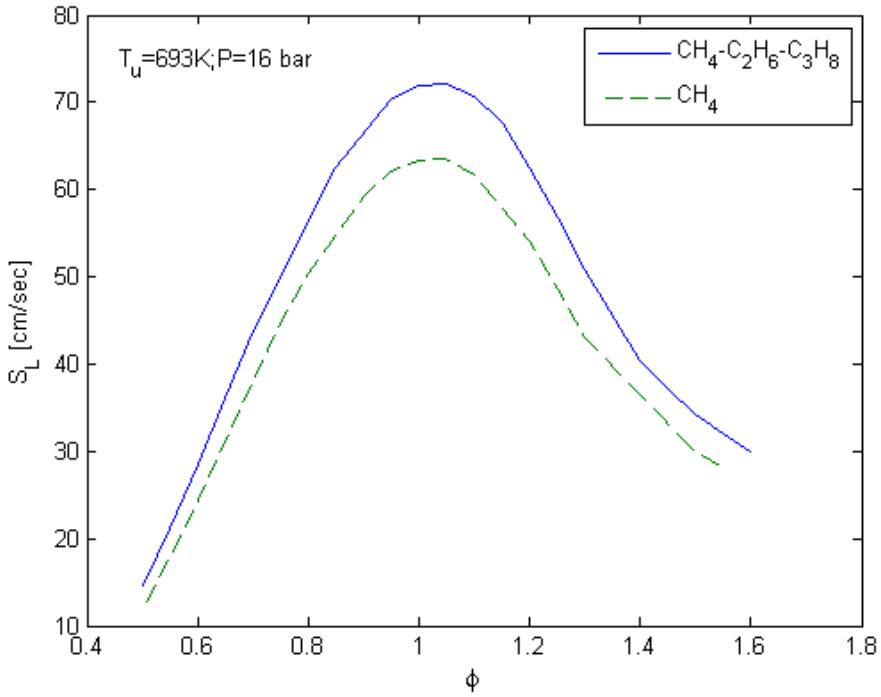

Figure 1. Laminar flame speed as a function of equivalence ratio of Standard Natural Gas Approximation compared to pure methane, both burning in air at P=16 bar with a preheat temperature Tu=693K.Key: Solid – methane-ethane-propane; Dashed – methane.

C Calculating the Global Chemical Time Scale

```
function [tau_chem,Tf,dL] = chemtime(S_L,T,x)
%Calculates the approximate global chemical time scale for a premixed
%laminar flame with temperature profile T with velocity profile S_L at
%gridpoints x
%-------------------------------------------------------------------

[dL,Tf] = flamethickness(x,T);
tau_chem = dL/S_L;


function [dL,Tf] = flamethickness(x,T)
%Calculates the flame thickness of a laminar premixed flame with
%temperature profile T with corresponding gridpoints x using the FWHM
%approach
%-------------------------------------------------------------------

Tf = T(length(T),1);
%Calculate the gradient of T
dT = grad(T,x);

%Find maximum gradient and position
[maxdT, maxpos] = max(dT);

for i = 1:maxpos
    if dT(i) == 0.5*maxdT;
        dL1 = x(maxpos) - x(i);
    end
    if dT(i+1) > 0.5*maxdT & dT(i) < 0.5*maxdT  %Linear interpolation
        dL1 = x(maxpos)-x(i)-((0.5*maxdT)-dT(i))*((x(i+1)-
x(i))/(dT(i+1)-dT(i)));
    end
end
for i = maxpos:length(dT)-1
    if dT(i) == 0.5*maxdT;
        dL1 = x(i) - x(maxpos);
    end
    if dT(i+1) < 0.5*maxdT & dT(i) > 0.5*maxdT  %Linear interpolation
        dL2 = x(i) - x(maxpos) + ((0.5*maxdT)-dT(i))*((x(i+1)-
x(i))/(dT(i+1)-dT(i)));
    end
end

dL = dL1 + dL2;


function [dy] = grad(y,x)
%Calculate gradient at each point in y using CD approximation assuming
zero
%gradient boundaries
%-------------------------------------------------------------------
-----
dy = zeros(length(y),1);

for i = 2:length(y)-1
    dy(i,1) = (y(i+1)-y(i-1))/(x(i+1)-x(i-1));
end
```

D Preheat Temperature For Ignition

The appropriate preheat temperatures to induce auto ignition are defined based on the critical flow residence time where flameback might be induced; $\tau_{ig} = t_{c,3} \cong \frac{L_f}{u_{in}}$

The flame position is assumed to approximately equal to the mixing tube length of the LB000 reference burner used in the rig tests, hence $L_f \cong 0.3m$. The flow velocity in the mixing tube is approximately $u_{in} \cong 85-90$ m/sec yielding:

$$\tau_{ig} = t_{c,3} \cong \frac{L_f}{u_{in}} \cong \frac{0.3}{85} - \frac{0.3}{90} \approx 3.3-3.5m\,\text{sec}$$

Simulations of ignition delay as a function of preheat temperature for a pure natural gas fuel mixture was performed and the results are shown below:

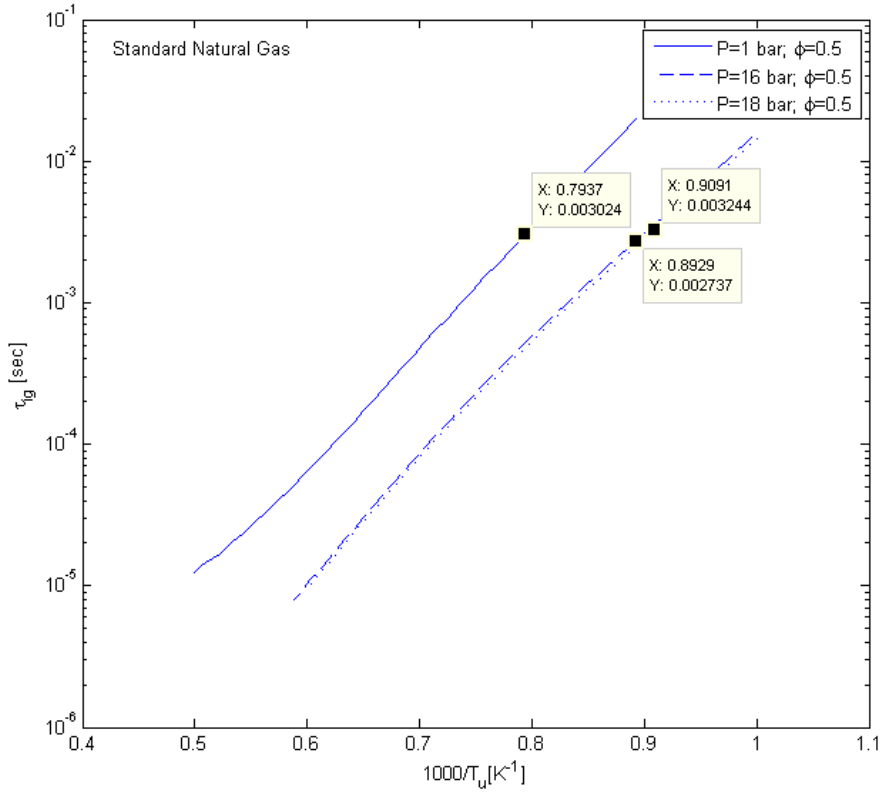

Figure 1. Ignition delay as a function of preheat temperature Tu for 3 different pressures at an equivalence ratio of 0.5

From the graph above approximate preheat temperatures were chosen as:

P=16bar Tu=1100K
P=18bar Tu=1100K
P=1bar Tu=1250K